

# A Review on Active 3D Microstructures via Direct Laser Lithography

Irene Bernardeschi,\* Muhammad Ilyas, and Lucia Beccai\*

Direct laser lithography (DLL) is a key enabling technology for 3D constructs at the microscale and its potential is rapidly growing toward the development of active microstructures. The rationale of this work is based on the different involved methodology, which is referred as indirect, when passive microstructures become active through postprocessing steps, and direct, when active structures are directly obtained by fabricating microstructures with active materials or by introducing heterogeneous mechanical properties and specific design. An in-depth analysis of both indirect and direct methods is provided. In particular, the wide range of materials and strategies involved in each method is reported, including advantages and disadvantages, as well as examples of fabricated structures and their applications. Finally, the different techniques are briefly summarized, and critically discussed by highlighting how the new synergies between DLL and active materials are opening completely new scenarios, in particular for sensing (e.g., mechanical) and actuation at the microscale.

resolutions reaching 10 nm and below.<sup>[18–20]</sup> However, such techniques are limited to 2D or 2D and a half-dimensionality, or in 3D they allow fabrication of simple geometries, mainly requiring a multistep fabrication process using sacrificial layers. More complex 3D designs can be achieved with 3D printing technology, but with lower resolution.<sup>[21–23]</sup>

In DLL, a photosensitive resin changes its solubility to a developing agent (polymerization or decomposition) if irradiated with an amount of energy able to induce the absorption of photons. This is possible when a femtosecond (fs)-pulsed long wavelength laser is highly focalized in a small volume of material (voxel) because multiphoton absorption is a nonlinear process and the required energy scales with the square of the irradiated energy (or more

in case of more than two-photon adsorption). Thus, the rest of material is transparent to the laser light, and moving the laser focus inside the material itself allows fabricating real 3D intricate structures.<sup>[24,25]</sup> However, 3D submicron structures have been successfully obtained with DLL by using a continuous-wave laser and one-photon absorption.<sup>[26–28]</sup> In DLL the laser is then focalized in the photosensitive material by passing through a high numerical aperture objective and 3D microstructures can be obtained by scanning the laser focus inside the material. This can be obtained by scanning either the laser focus relative to the sample or vice versa, through a mirror system using galvanometric scanners or by using a movable stage, respectively.<sup>[16,29,30]</sup> **Figure 1** shows a simplified schematization of DLL equipment.


The wide applicability of DLL depends strongly on the materials made available for fabrication; therefore, quite a few have been developed,<sup>[31]</sup> and optimized for improving resolution and feature size. In this route, today DLL is undergoing a shift as it is assuming a core role not only for developing passive microstructures (with all the aforementioned characteristics), but as a unique enabling technology for fabricating structures capable of transducing a stimulus or of implementing motion at the microscale, and here referred as active microstructures. This is opening completely new scenarios for sensing (in particular, force sensing) and actuation, for which active 3D layouts are needed as core elements for implementing transduction or motion, respectively.

This review aims at identifying and categorizing different approaches for building active 3D microstructures, highlighting the potential of DLL in this manufacturing field. To this aim, the

## 1. Introduction

The development of 3D structures at the microscale represents an important requirement in various fields such as tissue engineering and cell biology,<sup>[1–4]</sup> photonics, plasmonic and metamaterials,<sup>[5–7]</sup> micro electro-mechanical systems (MEMS),<sup>[8,9]</sup> drug delivery,<sup>[10,11]</sup> biomimetics,<sup>[12,13]</sup> and microfluidics.<sup>[14,15]</sup> In the recent past, direct laser lithography (DLL) has gained great attention for building 3D structures of high architectural complexity. Also known as direct laser writing (DLW), it is a powerful and reliable technique enabling precise and high-resolution (below 100 nm) fabrication.<sup>[16,17]</sup> Noteworthy, the previous aspects cannot be achieved by other single fabrication approaches. For example, extreme ultraviolet lithography (EUVL), focused ion beam or e-beam lithography (FIBL or EBL) or other next-generation lithographic techniques enable very small feature sizes with

Dr. I. Bernardeschi, Dr. M. Ilyas, Dr. L. Beccai  
Soft BioRobotics Perception Lab  
Istituto Italiano di Tecnologia  
Via Morego 30, 16163 Genova, Italy  
E-mail: irene.bernardeschi@iit.it; lucia.beccai@iit.it

 The ORCID identification number(s) for the author(s) of this article can be found under <https://doi.org/10.1002/aisy.202100051>.

© 2021 The Authors. Advanced Intelligent Systems published by Wiley-VCH GmbH. This is an open access article under the terms of the Creative Commons Attribution License, which permits use, distribution and reproduction in any medium, provided the original work is properly cited.

DOI: 10.1002/aisy.202100051

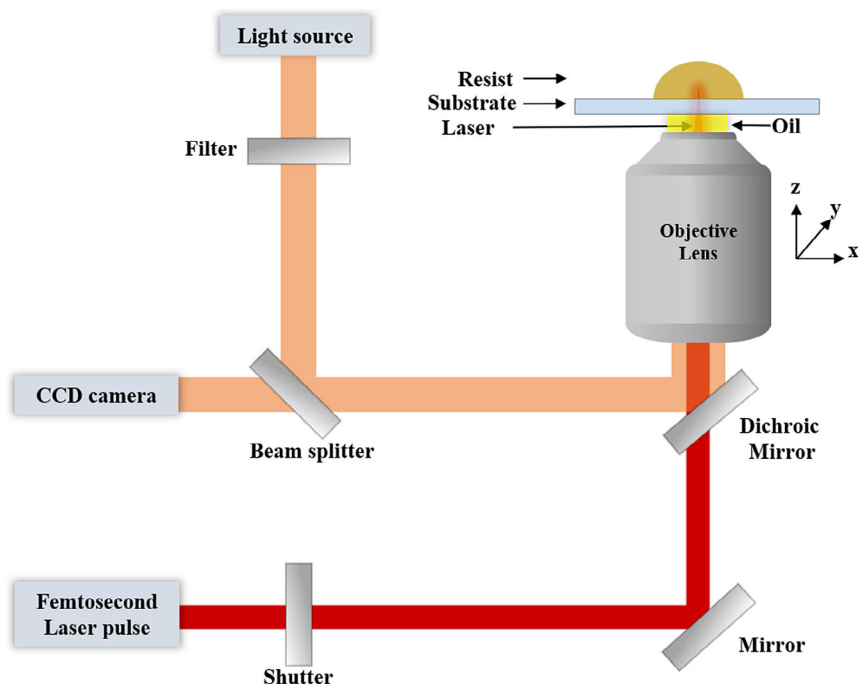


**Figure 1.** Simplified schematic of a Direct Laser Lithography (DLL) system.

fabrication strategies are grouped as either indirect or direct approaches. Indirect methods involve two-step fabrication processes in which DLL is mainly used in the first phase for developing a passive structure with desired design. The second step is a postprocessing phase in which the structure is modified to make it active, or used either as template for depositing active materials or as master for replica molding. Instead, direct methods involve the use of materials with specific and custom properties to be processed by DLL for directly having an active microstructure, also by tuning of geometry and writing parameters. For each approach, different strategies can then be adopted in association, and **Figure 2** shows a schematic overview.

In the next sections, an in-depth analysis of both indirect and direct methods is provided. In particular, the wide range of materials and strategies involved in each method is reported, including advantages and disadvantages, as well as examples of fabricated structures and their applications. Finally, the different techniques are briefly summarized, and critically discussed by giving indications about the possible more suitable specific strategies to adopt depending on the application-driven requirements.

## 2. Indirect Fabrication

Active microdevices are often built by a dual-step fabrication process. At first, a passive structure is realized by using commercial photosensitive materials that are optimized to best express the potentialities of DLL. Then, the obtained structure becomes functional or active, adding materials (conductive, magnetic, etc.) such as metal layers, metal NPs, or conductive polymer molecules. In some cases, biological components can also be used, and associated with artificial passive microstructures in a

biohybrid approach, for exploiting their natural functionalities. Passive hollow structures can also be used as templates and molds for active materials growth or casting, or as masters for replica molding.

In the following sections, different indirect methods are described, highlighting some specific studies, whereas a comprehensive literature classification is provided in Table S1, Supporting Information.

### 2.1. Modification of Passive Microstructures

In the aforementioned dual-step processing, passive microstructures are subjected to postprocessing treatments to make them active. The postprocessing involves deposition or adsorption of conductive/magnetic materials, or integration of biological components. This approach is mainly required for applications in which complex 3D geometries, high resolution, and/or precise control of dimensions at the microscale are strictly required. Therefore, DLL can be exploited to its full potential because structures can be fabricated with commercial photosensitive materials in a single fabrication step.

#### 2.1.1. Deposition of Metal Layers

Metal layers deposition involves covering selected regions of the structure surface with layers of conductive/magnetic materials by means of metal deposition techniques such as sputtering,<sup>[32–41]</sup> e-beam evaporation,<sup>[42–48]</sup> spray coating,<sup>[49]</sup> and physical vapor deposition.<sup>[50–52]</sup> The fabrication of a sacrificial structure to be removed after the deposition process is often required to deposit the material only on the desired surface (i.e., head of a microrobot).<sup>[32]</sup>



microswimmer, composed of rigid segments connected by joints, is fabricated by DLL with IP-L 780 photoresist (Nanoscribe, GmbH) (**Figure 3a**). Such microscale device (total length and height of 120 and 16  $\mu\text{m}$ , respectively, a head width of 4  $\mu\text{m}$ ) can be guided magnetically owing to a 100 nm Ni layer deposited (by sputtering) on its head. Here, the complex geometry is functional to the motion capabilities of the microswimmer because the oscillation of the magnetic head induced by the external magnetic field is transmitted to all the other segments

through a U-type connection, generating traveling wave propulsion. Furthermore, the high resolution of the fabricated structures allows the smooth transmission of the movement among the links, achieving structural flexibility.

Indeed, other capabilities (e.g., color expression) have also been demonstrated recently in magnetic microrobots owing to DLL potential. Koepele et al.<sup>[47]</sup> present a magnetically actuated 3D microstructure, composed of a helical tail (100  $\mu\text{m}$  length) connected to half-cylindrical (20  $\mu\text{m}$ ) head. The latter has a

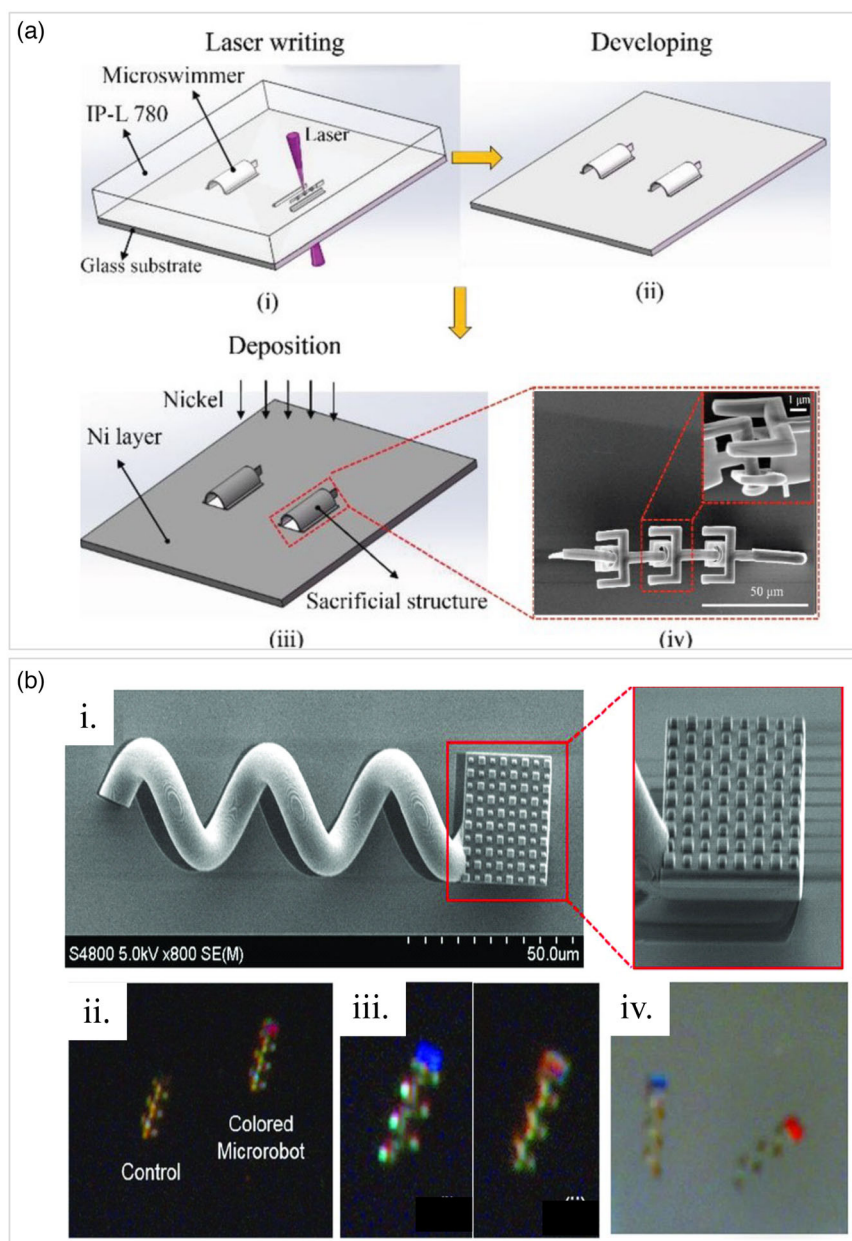


**Figure 3.** a) Fabrication process of the microswimmer. In the red square SEM image of the microrobot without the sacrificial structure and detail of the U-type connection. Reproduced with permission.<sup>[32]</sup> Copyright 2019, Wiley-VCH Verlag GmbH & Co. KGaA, Weinheim. b) (i) Scanning electron microscope (SEM) image of helical microrobot with a color-expressing pattern area located on the top surface of the helix head; (ii) helical microrobot with integrated structural red and control microrobot with no patterns; (iii) color expressed at low (blue) and high (red) frequencies; (iv) two colored helical microrobots with different nanopatterns expressing different colors. Reproduced with permission.<sup>[47]</sup> Copyright 2020, Wiley-VCH Verlag GmbH & Co. KGaA, Weinheim.



surface structured with an ordered array of high-resolution micropillars with a prismatic shape pointing upward (Figure 3b(i)). All the microstructure is realized by means of DLL and IP-Dip photoresist (Nanoscribe, GmbH) in a single fabrication step. A Ni 100 nm layer coated on top serves the magnetic navigation, while an additional 35 nm layer of Ge deposited by e-beam evaporation is used as a color enhancer (i.e., increase color contrast). The surface patterns express specific colors (i.e., red and green or a combination) depending on spacing, size, and shape of the nanostructures. Also, they change with the relative position (angle) of the microrobots (achieved via a magnetic rotating field) with respect to a fixed white light source having constant intensity. Noteworthy, the color change can be used as a sensor during navigation because it can provide real-time information on the microrobot's position in the 3D workspace (Figure 3b(ii)–(iv)). Here, geometry and materials are important for microrobot's operation for tasks such as targeted delivery: the helical tail covered with magnetic material enables efficient propulsion for navigation in a complex environment, and the specific head nanostructure, and material, provides a mean for visual tracking.

The combination of DLL and metal layer deposition enables efficient propulsion at the microscale not solely in the case of external magnetic fields, but also by triggering catalytic reactions with components present in the local environment, in which a microrobot is supposed to navigate. In this scenario, the bubbles formed as a consequence of the chemical reaction are used as propellers, like in the work of Chen and coworkers<sup>[43]</sup> where a 4 nm-thin Pt layer is e-beam deposited in the inner cavity of microtubular structures fabricated through DLL using IP-Dip photoresist. When microtubules are immersed in a hydrogen peroxide solution, the Pt layer acts as catalyst decomposing the H<sub>2</sub>O<sub>2</sub> in oxygen and H<sub>2</sub>O, thus generating bubbles that, ejected from inside the hollow structure, cause the propulsion of the microstructures. While microtubules' speed is enhanced by bubbles' expulsion frequency, the same is also increased by adopting a more complex microstructure design, indicating the fundamental role of geometry in controlling the motion parameters. Furthermore, the dual-step processing using metal layers can play a key role in the fabrication of unique sensing microstructures. This is the case of force microsensors that can be used in vivo, where contact with soft biological tissues requires soft sensors with enhanced sensitivity, and specific detection ranges, to not damage the tissues. For example, in the work of Li et al.<sup>[49]</sup> a force microsensor is developed by exploiting the versatility of 2PP associated with the deposition of carbon nanotubes (CNTs). Microsprings in different configurations are fabricated through DLL using IP-S photosensitive resin, and then converted to conductive by spray coated CNT networks to achieve a resistive transducer. The sensor configuration with functional springs and a suspended Au electrode is shown in **Figure 4a**. When a force is applied, the electrode touches the functional spring creating a closed circuit with an increase in current that varies with spring compression (Figure 4b). With this approach, different force sensing ranges and sensitivities can be obtained by modifying the geometry and number of the springs (Figure 4c,d). For example, using an array of functional springs with different lengths enables multiple step sensing and this mechanism can be potentially used for applications requiring

a working condition under controlled force (e.g., a surgical tool holding a tissue with a force large enough just to make contact but avoiding tissue damage). Here, the geometry and materials are associated with the advanced functionality of soft sensors both in vivo and in vitro. The high control on spring geometry and length scale by DLL allows tuning sensitivity and force range, while the materials such as CNTs enable the resistive transduction principle.

### 2.1.2. Nanomaterials or Conductive Polymers Molecules Adsorption or Chemical Link

Passive microstructures can be turned into active also by adsorbing or chemically linking conductive or magnetic materials, usually in the form of NPs or conductive polymers' molecules.<sup>[53–56]</sup> For example, in the work of Dong and coworkers<sup>[54]</sup> magnetoelectric nanoparticles (MENPs) are adsorbed on the surface of 3D printed biodegradable helical structures for neuronal cell delivery and stimulation, by incubation in a water solution, forming a uniform layer. The resulting microswimmers rotate (due to magnetic field) along their long axis in a corkscrew motion at low frequency, with a swimming velocity increasing with the length. MENPs can also be used for inducing differentiation of neuronal cells under electrostimulation because they can convert magnetic input into an electric output. In another example,<sup>[53]</sup> 3D helical biodegradable microswimmers are fabricated by laser polymerization of gelatin methacryloyl (GelMA) and made magnetic by incubation in aqueous suspensions of magnetite (Fe<sub>3</sub>O<sub>4</sub>) NPs, as shown in **Figure 5a**.

Self-propelled microswimmers can also be fabricated by selectively linking conductive NPs in some specific portion of passive microstructures. To this aim, Ceylan and coworkers<sup>[56]</sup> exploited two-photon absorption for, both, fabrication of the passive structures and subsequent selective patterning. Indeed, in the first step a 3D bullet-shaped low drag structure is fabricated using PEGDA by DLL having an inner cavity with an open small nozzle. Then, the structure is swollen with a second photoinitiator-containing 2-carboxyethyl monoacrylate (R1) solution. The microcavity is then selectively laser exposed again—triggering the cross-linking reaction between PEGDA and R1, and the consequent patterning of carboxylic acid groups. The latter are converted to sulfhydryl groups allowing the nucleation, and growth, of Pt NPs only in the engine site. Jet bubbles are generated in the cavity because of the catalysis induced by Pt on H<sub>2</sub>O<sub>2</sub>, and are expelled through the nozzle inducing the self-propulsion of the structure. In this example, DLL is used for both fabrication and subsequent selective patterning of the structure for obtaining the desired final functional properties, i.e., a self-propelled microswimmer.

Conductive polymer molecules are also used, with multiwall nanotubes (MWNTs) to achieve highly conductive (0.1–42.5 S m<sup>-1</sup>) 3D hydrogels.<sup>[55]</sup> The structures are fabricated using a MWNTs-doped photo-curable material processed with two-photon hydrogelation, generating nanostructured electrically conductive hydrogels (NECHs) with chemical functional groups and lateral features size down to 200 nm. Conductivity is enhanced by the self-assembly of PEDOT:PSS into the unfolded polymeric matrix with water diffusion process, and PEDOT interacts with MWNTs by noncovalent bonds, increasing the

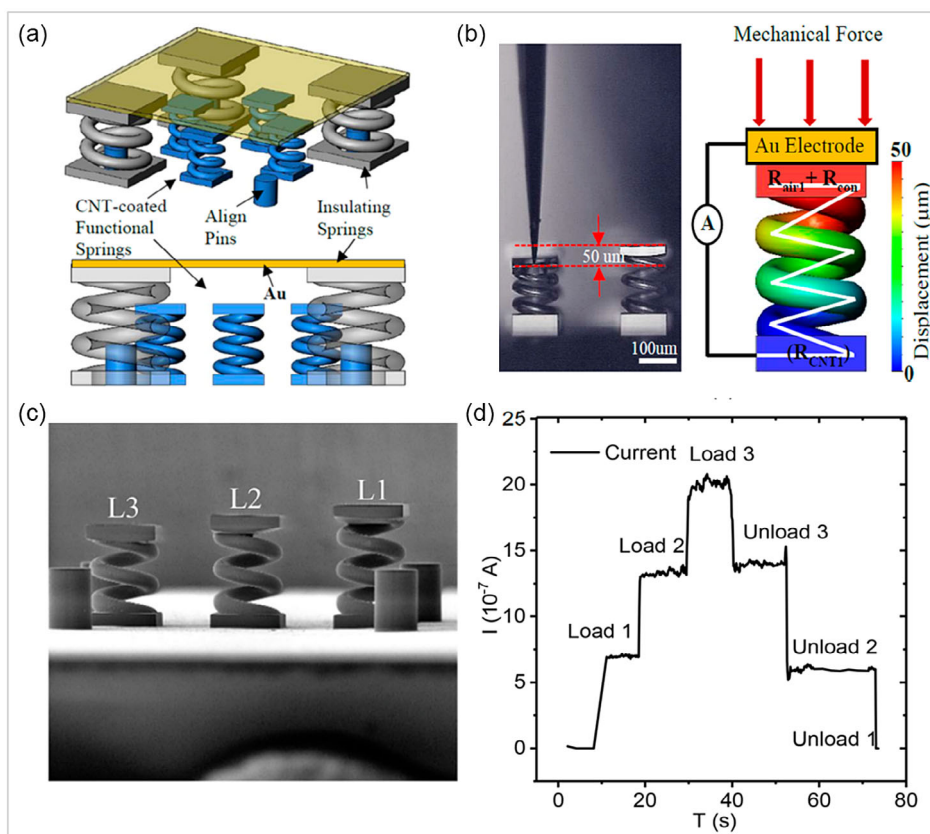


**Figure 4.** 3D force microsensors. a) Tilted and front view of the design with supporting springs (gray), functional springs (blue), and Au electrode (yellow). b) The application of a force causes the electrode to touch the spring creating a closed circuit with a measurable current change. c) SEM image of three steps force microsensors. d) Current output signal during complete loading and unloading cycle of the three steps force microsensors. Reproduced with permission.<sup>[49]</sup> Copyright 2019, American Chemical Society.

conductivity of the structure (Figure 5b(i)). Many 3D electrically conductive microscale structures such as photonic crystals, interdigitated capacitors, loop spiral-like inductors, and so on are fabricated efficiently with this process (Figure 5b(ii)–(iv)), showing optical clarity, high conductivity, and extensibility due to the combination of polymers and carbon-based materials properties in a predefined 3D structure.

### 2.1.3. Biohybrid Approach

Another strategy for achieving active structures from passive ones is the biohybrid approach, which consists in the integration of artificial constructs and biological components. For example, self-propelling living microorganisms such as bacteria or ciliated cells can be encapsulated in artificial structures fabricated with DLL and exploited as a means for propulsion. Self-propelled cells are attractive for applications as targeted drug delivery systems, due to their ability to interact with other cells/tissues, and their optimal swimming capabilities in physiological microenvironments. In the works of Xu et al.,<sup>[57,58]</sup> a new type of sperm-hybrid micromotor is proposed for potential application in targeted drug delivery. A smart tetrapod microstructure is designed to have a tubular body and four flexible arched arms spaced  $4.3\ \mu\text{m}$  (Figure 6), able to capture bovine sperm cells which have an

average  $4.5\ \mu\text{m}$  wide head. The tetrapod microstructure is fabricated with IP-Dip photoresist. While the encapsulated sperm cell is used for propelling the microstructure, a 10 nm layer of iron is deposited asymmetrically on the surface of the passive structure to guide it using an external magnet (an additional 2 nm Ti layer of is added to improve the system biocompatibility). In the proposed system, the efficiency of drug delivery is strictly related to the smart design of the passive structure. Indeed, when the structure comes in contact with targeted cells (i.e., HeLa cells) the arms bend allowing the release of the sperm cells that are then able to contact the cells and deliver the loaded drug. Thus, the control on dimensions and geometry plays a key role in this kind of application: tetrapods with a slightly different distance among the arms can prevent the efficient encapsulation of the sperm cell, or cause the premature release of the sperm cell before reaching the targeted cell.

## 2.2. Templates, Molds, and Masters

Complex templates can be fabricated with DLL for being used for the electrodeposition or casting of conductive/magnetic materials<sup>[5,6,59–65]</sup> or as masters for the replica molding of active materials.<sup>[66,67]</sup> With this approach the limitation related to the use of photocurable materials is outdated, and microstructures can be achieved with active but not photosensitive materials.

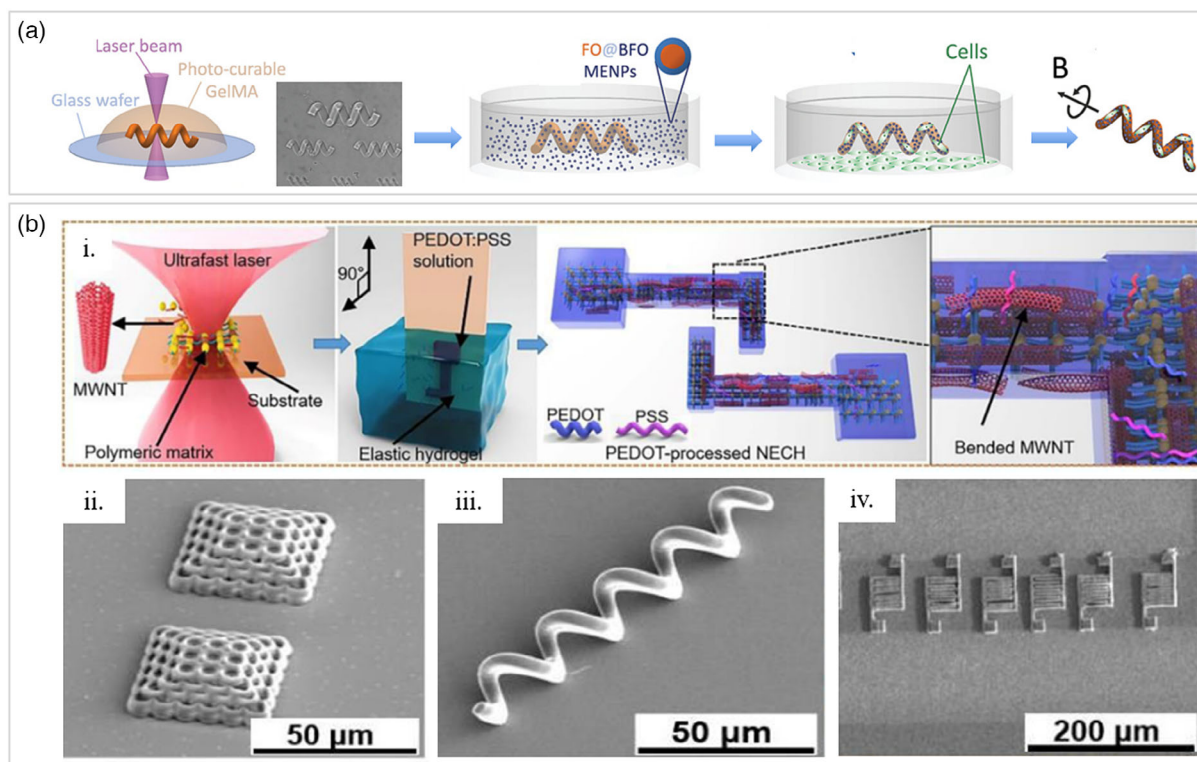


**Figure 5.** a) Schematic of the fabrication process of biodegradable soft helical microswimmers: (i) DLL process; (ii) incubation of the microstructures in a magnetite NPs aqueous suspension; (iii) optical image of microswimmers with adsorbed magnetic NPs; (iv) energy dispersive X-ray analysis (EDX) of hydrated microswimmer mapping the presence of iron. Reproduced with permission.<sup>[53]</sup> Copyright 2018, John Wiley and Sons. b) (i) Schematic of the two-photon hydrogelation with DLL of the MWNTs containing hydrogel and consequent incubation and self-assembly of PEDOT:PSS by noncovalent interaction and hydrogen bonding with MWNTs; (ii) photonic crystals; (iii) spiral-like inductor; (iv) microinterdigitated capacitors. Reproduced with permission.<sup>[55]</sup> Copyright 2019, The Royal Society of Chemistry.

### 2.2.1. Templates and Molds for Electrodeposition or Casting of Active Materials

Electrodeposition has been extensively used for the fabrication of photonic crystals and metamaterials for optical applications.<sup>[5,6,64]</sup> Metal is grown in a plating solution through a template starting from the conductive base on which it is fabricated (Figure 7a). At the end of the process, the template is removed by using the proper removal solution or oxygen plasma etching. This microfabrication process can strongly benefit from DLL because templates of different and complex geometry can be fabricated for obtaining metal structures of any 3D shape for many applications.

For example, magnetic materials can be electrodeposited for fabricating magnetically actuated structures.<sup>[59–63]</sup> In the work of Alcantara et al.,<sup>[63]</sup> the chemically amplified positive photoresist AZ IPS6050 is used to fabricate templates for the electrodeposition of iron from a mixed ferrous sulfate–chloride electrolyte solution. In this case, the 3D mold is fabricated using a modified writing configuration, which overcomes previous limitations such as the use of transparent substrates, low writing speeds, and limited depth of field. The positive-tone photoresist is immersed in a refractive index-matching elastomer directly in contact with the objective. As there are no limitations in the

substrate choice, highly conductive layers could be used to be directly used as working electrodes for electrodeposition. In this way, magnetic microstructures actuated by an external magnetic field can be obtained in many different and complex shapes, starting from a mixed ferrous sulfate–chloride electrolyte solution (Figure 7b). As an example, a 5turn helix with 25 μm radius and 20 μm pitch showed a maximum velocity of 42 μm s<sup>−1</sup> in the presence of applied rotating magnetic fields.

The specific design with multiple contacts with the conductive surface (Figure 7b(i)) obtained via DLL also facilitates the gas release, allowing the smooth growth of the material without porosity or embrittlement caused by the formation of H<sub>2</sub> bubbles during the deposition process. The iron-based microrobots fabricated with this process exhibit a high magnetic torque and are biocompatible, thus enabling their use in biomedical applications.

In another research work, the template is directly used as a mold and filled with stimuli-responsive UV-curable materials for having active structures responding to specific external stimuli such as temperature variation.<sup>[65]</sup> In another work of Alcantara,<sup>[68]</sup> DLL has been used for the fabrication of structures used as both templates for electroplating and molds for polymer casting for achieving multimaterial structures composed of combined metal and polymers. The only constraint consists in

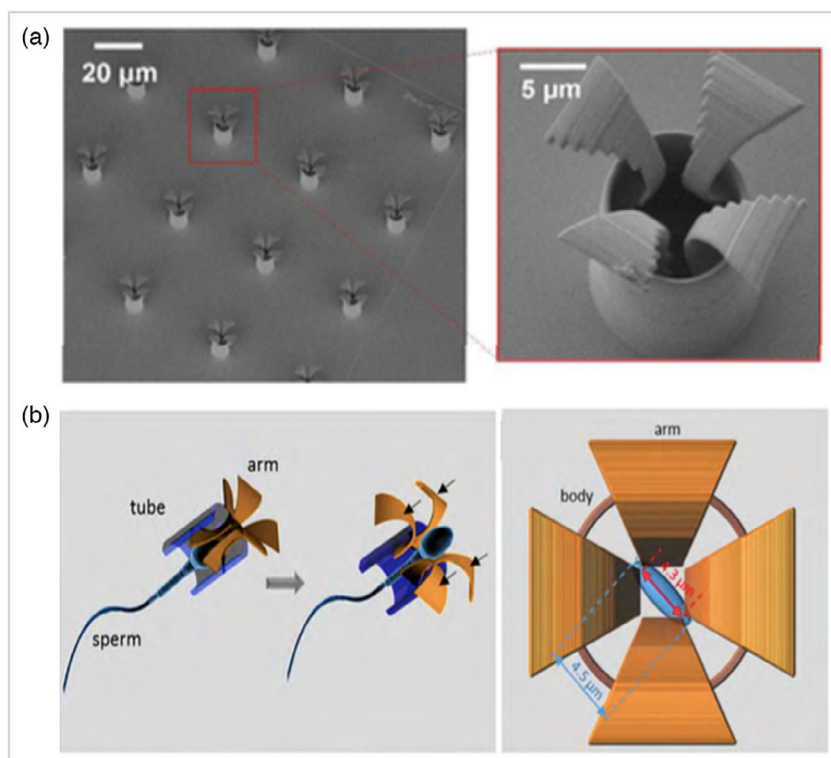


**Figure 6.** a) SEM images of smart tetrapod microstructures with tubular body and four flexible arched arms. b) Schematic illustrating the mechanical release mechanism. Reproduced with permission.<sup>[57]</sup> Copyright 2017, American Chemical Society.

designing geometries that do not overlap for the different deposition strategies. This way, interlocked metal-organic structures can be obtained with enabled complex actuation mechanisms. Also, independent 3D shapes can be built in either electrodeposited metal or casted polymer that does not influence each other. Therefore, the advantages of having either a full metal structure (e.g., enhanced magnetic performance) or flexible microstructures (e.g., in shape-memory polymers, silicon-based elastomers, etc.) can be exploited for different applications.

### 2.2.2. Masters for Replica Molding

DLW is used for the fabrication of masters for obtaining active structures through the replica molding process.<sup>[66,67]</sup> Usually, polydimethylsiloxane (PDMS) or other silicone materials are used for the mold fabricated from the master and used for casting active materials. In this way, the designed master structure fabricated with DLL is reproduced with nonphotosensitive active materials. This is the case of the work of Fiorello et al.,<sup>[66]</sup> in which a thermoplastic polymer (i.e., polycaprolactone [PCL]) filled with gold NPs (Au NPs) is shaped reproducing rose-inspired prickle-like hooks (Figure 7c). When exposed to infrared laser light, the heat generated by the irradiated Au NPs inside the thermoplastic matrix alters the stiffness of the polymer (i.e., less stiff when irradiated) allowing the control of hold and release of a small weight. In this case, IP-S photoresist (Nanoscribe, GmbH) is used for fabricating the master prickle-like hook microstructure.

## 3. Direct Fabrication

Active structures can be directly fabricated with DLL by using materials with specific properties. This involves the modification of passive photosensitive materials by mixing metal NPs or other conductive materials such as ILs, or by adding metal precursors exploiting the energy of the laser to induce photoreduction of metal ions to metal NPs, or by using metal-rich photoresists. Solutions of metal ions or metal oxide NPs can also be used to directly obtain metal structures. However, also mechanical properties have a fundamental role in achieving active devices, and they can be modified by, e.g., incorporating materials with different stiffness, designing smart geometries, or inducing cross-linking gradients in the integrated stimuli-responsive materials (by ad hoc modifications of writing parameters) to elicit specific responses of the active structures.

As direct fabrication methods, the two main aforementioned strategies are described in the next sections. Some specific and most recent studies are highlighted, and a comprehensive literature classification is provided in Table S2, Supporting Information.

### 3.1. Modification of Passive Photocurable Materials

Photocurable passive materials can be modified for achieving active microstructures by mixing components such as magnetically<sup>[69–72]</sup> or electrically<sup>[73,74]</sup> conductive NPs, ILs,<sup>[75–77]</sup> or metal precursors<sup>[78–82]</sup> into the resin before DLL fabrication. Unlike the



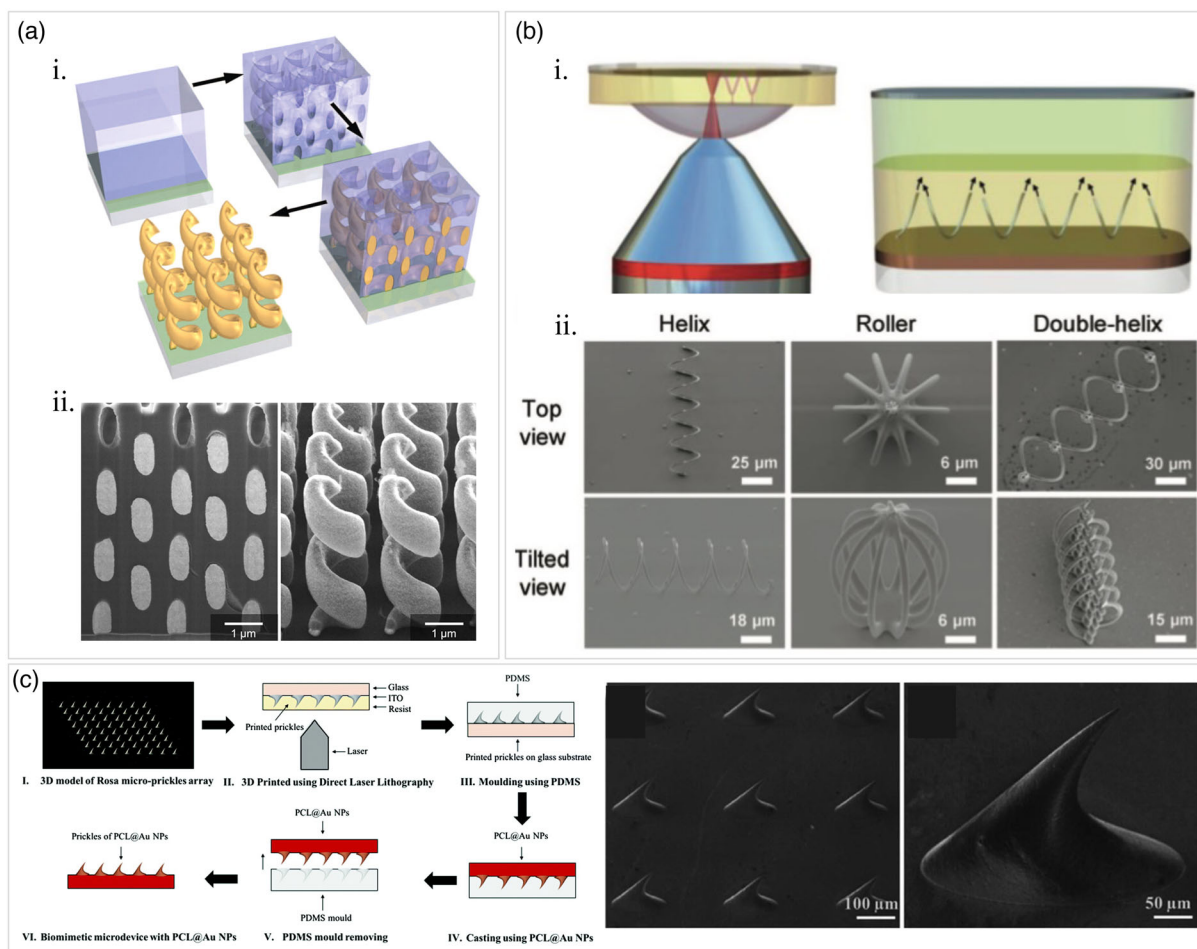


**Figure 7.** a) (i) Positive-tone photoresist (blue) deposited on a glass substrate covered with a conductive thin layer of indium tin oxide (ITO, in green) is exposed to DLL and then developed obtaining an array of excavated helices used for gold electroplating. The removal of the polymeric template by plasma etching leaves an array of 3D gold freestanding helices. (ii) SEM image of the side view of a partially filled template and oblique view of 3D gold helices obtained after template removal. Reproduced with permission.<sup>[5]</sup> Copyright 2009, The American Association for the Advancement of Science. b) Schematic of the fabrication process of iron microstructures. The chemically amplified positive-tone photoresist (AZ IPS6050) directly contacts the objective of a DLL system immersed in a refractive index-matching elastomer. The specific design with multiple contacts with the conductive surface facilitates the gas release allowing the smooth growth of magnetic iron structures through the electrodeposition from a mixed ferrous sulfate–chloride electrolyte solution. (ii) SEM images of obtained high resolution complex microstructures. Reproduced with permission.<sup>[63]</sup> Copyright 2019, Wiley-VCH Verlag GmbH & Co. KGaA, Weinheim. c) Schematic of the microfabrication process of rose-inspired microdevice with prickle-like hooks arrays and SEM images of the fabricated rose prickles. Reproduced with permission.<sup>[66]</sup> Copyright 2019, Springer Nature.

indirect approach, the starting materials are modified before the fabrication of the desired structure is performed by DLL.

### 3.1.1. Mixing of Nanomaterials or ILs

Incorporating nanomaterials or ILs in the resin is a fast way to directly obtain active microstructures. The photosensitive properties allow them to remain entrapped into the polymer matrix after the laser-induced polymerization process. This kind of approach is used for applications in which the functionality is mainly related to the intrinsic properties of the material (induced by the presence of the fillers in this case). Some examples are the fabrication of electrodes or connections for which high conductivity is required, or when specific responses are needed

(e.g., increase in temperature localized in a very small volume for hyperthermia therapy), or when magnetic properties are exploited for actuation. In this context, Park and coworkers<sup>[69]</sup> fabricate magnetically actuated microrobots for performing active-controlled drug release and hyperthermia therapy. Helical structures with a diameter of 40  $\mu\text{m}$  and a length of 120  $\mu\text{m}$  are obtained through DLL by using a drug-containing superparamagnetic hydrogel composite prepared by mixing the photoinitiator Irgacure-369,  $\text{Fe}_3\text{O}_4$  MNPs (100 nm diameter), and an anticancer drug in a poly(ethylene glycol) diacrylate–pentaerythritol tetraacrylate (PEGDA–PETA) copolymer. The fabrication process is shown in **Figure 8a**. In this case, MNPs are used both for actuation, i.e., rotation of the helical microrobot around its long axis (by means of a rotating magnetic field), and hyperthermia therapy, i.e., conversion of electromagnetic into thermal

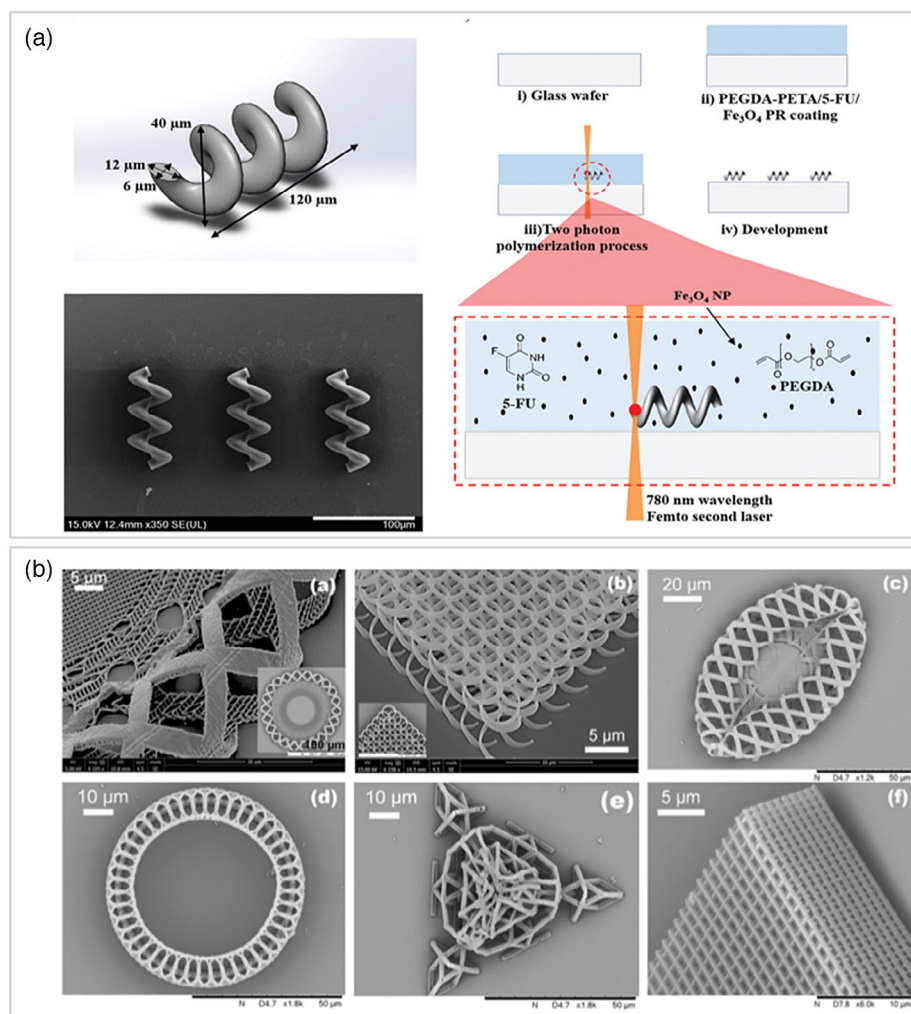


**Figure 8.** a) 3D design, fabrication method, and SEM images of magnetically actuated microrobots obtained through DLL by using a drug-containing superparamagnetic hydrogel composite. Reproduced with permission.<sup>[69]</sup> Copyright 2019, Wiley-VCH Verlag GmbH & Co. KGaA, Weinheim. b) SEM images of 3D high-resolution structures obtained via simultaneous two-photon polymerization and photoreduction of mixture composed of monomer, gold salt, and photoinitiator. Reproduced with permission.<sup>[78]</sup> Copyright 2017, Springer Nature.

energy (by applying an alternating magnetic field). In another work,<sup>[72]</sup> superparamagnetic iron oxide nanoparticles (SPIONs) are mixed to a chitosan-based photoresist, for fabricating with DLL a magnetically powered helical microswimmer for controlled drug release. Indeed, the free amino groups on the surface of the microstructure are chemically linked to photocleavable linker molecules through N-hydroxysuccinimide (NHS)–amine coupling. These molecules split in two parts when exposed to light, thus releasing the drug linked to them.

However, the addition of filler particles introduces some issues.<sup>[77]</sup> First of all, an increase in sedimentation of the particles can occur, and it must be considered in pursuing a final structure with homogeneous properties not only in terms of composition and, consequently, conductivity or magnetization, but also in terms of morphological properties. Indeed, the regions of the structure fabricated at the interface with the substrate will contain a higher concentration of particles because of the possible sedimentation over time. This phenomenon must be

controlled by adding solvents, and it can influence the photopolymerization process that must be properly tuned. Same issues are related to the possible inhomogeneous dispersion of the particles that can influence the properties of the final structure. For example, in the case of conductive structures, it has to be considered that the polymer matrix in which the particles are entrapped is an insulator, thus the conductivity strongly depends on the content of the conductive filler, following the known conductive composite behavior where a sufficient amount of filler is necessary to reach the percolation threshold.<sup>[83]</sup>

Moreover, particles can either scatter the laser light, causing a significant reduction in the structures' resolution, or they can absorb the power of the laser during the exposure, producing an amount of heat that can cause the burning of the photoresist.<sup>[80]</sup> The latter can be addressed by finely tuning the writing parameters, such as decreasing the repetition rate for lowering heat accumulation between consecutive pulses.<sup>[84]</sup> Another issue is represented by the low transparency of both uncured and

cured material that can be caused by the presence of the NPs, especially in case of high density, which leads to constraints in laser writing possibilities.

A possible solution to avoid the abovementioned issues is using ILs, which show high ionic conductivity and low volatility, excellent solvent solubility, and high thermal and chemical stability; they are transparent and many anionic/cationic combinations can be produced to tailor physical properties.<sup>[75–77]</sup> Such liquids are used both as solvent and as functional filler media for direct printing of all organic-based transparent and conductive 3D hybrid structures at the microscale. They represent an alternative to traditional conductive, yet brittle, inorganic materials such as In, Cd, and Sb oxides, providing flexibility and stretchability. As an example, Bakhtina et al.<sup>[75]</sup> report the fabrication of active 3D structures by DLL using 1-butyl-3-methylimidazolium dicyanamide IL and photoresist IP-G 780. The hybrid combination provides transparent electrodes with high conductivity ( $4 \times 10^{-7} \text{ S cm}^{-1}$  in a frequency range of 250 kHz–1 MHz) for application in soft transparent sensors, display devices, and electrical components.

### 3.1.2. Mixing of Metal Precursors

Passive photosensitive materials can be modified by exploiting the power of the DLL laser to induce the reduction of metal ions.<sup>[78–81]</sup> If metal precursors solutions are dissolved in a photosensitive material (e.g., solutions of metal salts such as  $\text{HAuCl}_4$  mixed to the liquid photoresist), the laser exposure will induce the photoreduction of the metal ions in parallel to the photopolymerization of the polymer. In a similar manner to 2PP, when the incident light intensity of the laser reaches a critical value, molecules in metal ionic solution undergo two-photon absorption to reduce the metal ions. The photoreduction process then causes the formation of metal NPs that remain entrapped in the polymer matrix forming a polymer–metal 3D microstructure. This technique offers the possibility to fabricate conductive structures with a high degree of design flexibility.

For example, geometrically complex structures containing Au NPs (Figure 8b) result from the simultaneous photopolymerization and photoreduction of a precursor photosensitive material composed of PETA with 0.5–1.5 wt% of 7-diethylamino-3-thenoylcoumarin (DETC) photoinitiator, and a second gold salt pre-resin containing gold(III) chloride hydrate ( $\text{HAuCl}_4 \cdot 3\text{H}_2\text{O}$ ) and 0.5–1.5 wt% DETC dissolved in *N,N*-dimethylacetamide (DMAC).<sup>[78]</sup>

An aspect to consider in choosing this method is that the resolution of the fabricated microstructures is related to the dimensions of the formed NPs: the lower the size of the particles, the higher the resolution, and also the surface roughness is lower. However, where needed, the resolution can be increased by using specific additives such as more efficient photoinitiators for controlling the photoreduction process.<sup>[78,80,85]</sup>

Some other issues concern low metal loading capability resulting in the formation of isolated aggregates of metal particles or low particle continuity, which can lead to the formation of structures having low conductivity because they are immersed in a dielectric polymer matrix.<sup>[85]</sup> Finally, as described in the previous section, the heat produced by the power absorbed by the formed

NPs can lead the solvents to reach the boiling point, causing the formation of bubbles which can destroy the microstructures, preventing the fabrication of structures with a defined and precise shape.<sup>[80,86]</sup> However, the heat accumulation can be decreased by decreasing the repetition rate of consecutive laser pulses but still enough to have sufficient average power for inducing simultaneous photoreduction and photopolymerization.<sup>[84]</sup>

Metal 3D microstructures can also be obtained by pyrolyzing metal-rich photoresists like described in the work of Vyatskikh et al.<sup>[82]</sup> Here, the hybrid organic–inorganic nickel acrylate is combined with an acrylic monomer (i.e., pentaerythritol triacrylate) and a photoinitiator (i.e., 7-diethylamino-3-thenoylcoumarin) for having a metal-rich photoresist, and then shaped in 3D by DLL. After washing away the nonpolymerized resist, the obtained structures are pyrolyzed to volatilize the organic content, and to consolidate Ni clusters, resulting in all-metal 3D structures with a very high resolution of 25–100 nm. This process can also be applied to other organometallics, and it can be used in the fabrication of 3D MEMS, 3D microbattery electrodes, and micro-robots. This last example describes metal structures obtained through a postfabrication process, the pyrolysis. However, it can be considered as a direct method because it involves the use of a modified photoresist containing a metal precursor, and the metal-containing 3D microstructure is directly fabricated by DLL. The pyrolysis is not used to modify a passive structure, rather to remove the organic component, and to consolidate the metal structure.

## 3.2. Direct Reduction of Metal Ions and Metal Oxide NPs from Solutions

Many additive manufacturing techniques are available to date for the fabrication of metallic 3D microstructures.<sup>[87]</sup> Among these, DLL allows to directly obtain full-metal 3D microstructures from solutions of metal ions and additional components, which can increase the efficiency of the process with an electroless plating fabrication process based on two-photon induced photoreduction.<sup>[85,86,88–92]</sup> In some cases, metal ions are dispersed inside solid supporting matrices (e.g., solutions of metal ions are mixed to polymer solutions before polymerization or are used to swell hydrogels) in which metal microstructures are created by DLL with the same photoreduction process.<sup>[93–96]</sup>

Solutions of metal oxide NPs are also used to directly obtain metal microstructures by the laser-induced reduction of the NPs.<sup>[97,98]</sup>

### 3.2.1. Metal ions Solutions

Fully metal structures can be directly fabricated starting from metal ions solutions, as reported by Tanaka et al. in 2006<sup>[86]</sup> for applications in MEMS or microelectronics. They obtain silver structures with conductivity only 3.3 times lower than bulk silver and micrometer resolution by two-photon-induced reduction of silver ions in an aqueous solution. Recent similar works show that nanometers resolution and smooth surfaces can be obtained starting from metal ions solutions by adding surfactants to be used as particle-growth inhibitor such as hexadecyltrimethylammonium bromide (CTAB), alkyl carboxylate (*n*-decanoylsarcosine

sodium [NDSS]), fatty salts (sodium valerate, sodium caprylate), and cetylpyridinium chloride (CPC), and trisodium citrate as a photo-reducing agent,<sup>[85,88–90,92]</sup> reaching conductivities of the same order of bulk gold.<sup>[85]</sup> Ren and coworkers<sup>[99]</sup> also demonstrate that by introducing amino acids in silver ions aqueous solutions, it is possible to reduce the power threshold required for triggering laser photoreduction while improving the conductivity. Indeed, they obtain silver nanowires (NWs) up to 25 times the conductivity of bulk silver and are able to reduce the structures linewidth by increasing scanner speed or decreasing laser power.

Metal ions solutions can also be mixed to polymer solutions before polymerization to obtain a solid polymer matrix with dispersed metal ions or can be used to swell hydrogels. In this way, when the laser is focused inside the solid polymer matrix<sup>[93–95]</sup> or hydrogel<sup>[96]</sup> in a DLL process, it induces the photoreduction of dispersed metal ions and metal microstructures with good conductivity are created inside the supporting structure.

### 3.2.2. Metal oxide NPs solutions

Femtosecond DLW is used for the direct laser-induced reduction of metal oxide NPs to form 3D metallic structures (i.e., laser reduction or direct writing) for application in pressure sensing, fluid flow sensing, and thermal detection.<sup>[97,98]</sup> This method is a fast, efficient, maskless direct writing process, executable at ambient atmosphere, thus surpassing other techniques such

as selective laser sintering (SLS) and e-beam melting (EBM) that operate under vacuum condition; or inkjet printing using only noble metal NPs (i.e., Ag and Au) as processable materials.

An example is reported in the study by Mizoshiri et al.<sup>[98]</sup> where a hot-film flow sensor with a Cu-rich microbridge heater is fabricated (**Figure 9**). The direct dispensing coating on a glass substrate of metal oxide solution composed of CuO NPs (42.1%), 2-propanol (41.1%), and polyvinylpyrrolidone (PVP) (16.8%) is followed by the laser-induced photoreduction of CuO NPs. The dispensing and laser patterning steps are performed until a final 3D structure with electrodes and a microbridge heater is obtained, and then the excess solution of nonreduced NPs is removed with ethanol.

The DLL process allows to control the degree of reduction of oxide NPs by adjusting the laser scanning speed, thus controlling the thermal energy transferred to the NPs for obtaining structures with good conductivity (i.e., resistivity is  $2.0 \times 10^{-5} \Omega \text{ m}$ ,  $\approx 104$  times larger than the bulk material). This permits to fabricate sensors with small dimensions and simple design like the bridge-like geometry that allows the system to not interfere with the fluid flow, thus having a flow sensor with high sensitivity.

### 3.3. Structures with Heterogeneous Mechanical Properties

Taking inspiration from nature it is possible to understand that the use of multiple materials with different mechanical properties can help to create complex actuation mechanisms

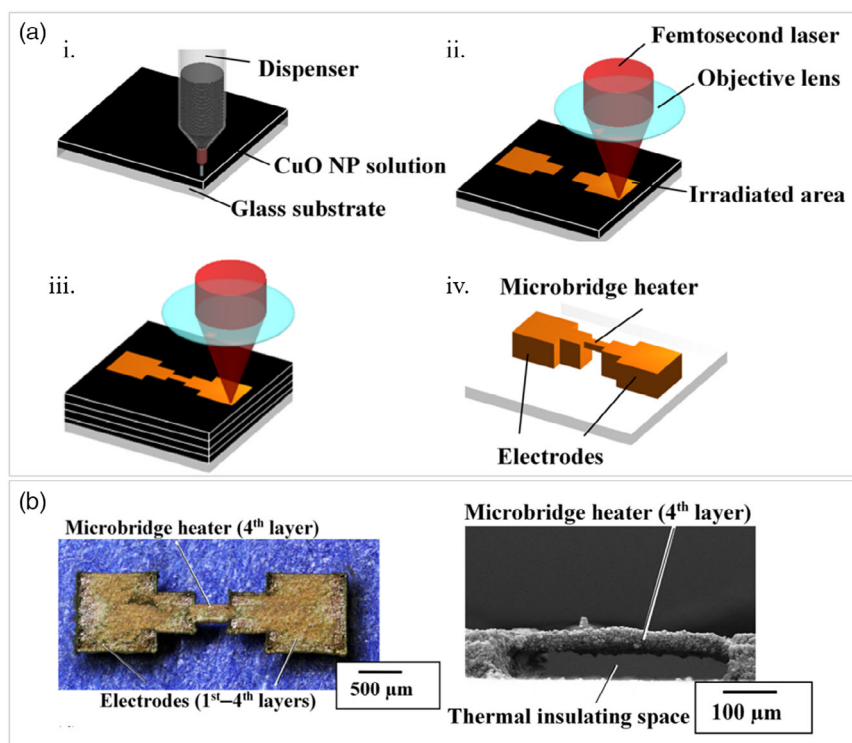


**Figure 9.** a) Schematic of the fabrication process of the flow sensor with a Cu-rich microbridge heater by laser-induced reduction of CuO NPs in solution: (i) dispensing of NPs solution on glass substrate; (ii) direct reduction of CuO NPs with fs laser; (iii) the structure is obtained by a layer-by-layer reduction process; (iv) removal of the excess solution and final structure with electrodes and microbridge heater. b) Optical image of the flow sensor with a Cu-rich microbridge heater and SEM image detail of the microbridge heater. Reproduced with permission.<sup>[97]</sup> Copyright 2016, The Japan Society of Applied Physics.



in very small volumes.<sup>[100]</sup> This can be obtained artificially by fabricating microstructures with DLL using two or more materials in a multimaterial approach. However, mechanical properties of a microstructure also depend on the cross-linking level of the used photosensitive polymeric material that can be easily modified by varying the laser writing parameters of the applied DLL process. If specific responsive materials are used, they will respond differently to the application of external stimuli based on the cross-linking level, creating complex actuation mechanisms. Another way to change mechanical properties in some parts of a microstructure is to play with geometry; in fact, even stiff resins can show a flexible/elastic behavior if shaped in specific high aspect ratio geometries, as in case of springs.

### 3.3.1. Multimaterial DLL

Soft and rigid materials can be integrated into the same microstructure by adopting a multimaterial DLL process.<sup>[101–103]</sup> Recently, Soreni-Harari and coworkers<sup>[101]</sup> demonstrated different structures composed of rigid parts connected through soft flexures (**Figure 10a**) by using either a soft elastomer (urethane diacrylate [UDA]) with  $E \approx 1$  MPa and the more rigid photopolymer IP-S, with  $E \approx 1$  GPa, in a two-step fabrication process, reaching 1  $\mu\text{m}$  resolution. The presence of soft elements properly integrated in a smart design allowed complex actuation mechanisms such as wings flapping in a mm scale 3D flapping structure, triggered by the deformation of six flexible joints due to the presence of a micromagnet in the structure and application of an external magnetic rotating field.

In multimaterial DLL, the main issue is the multistep process required for fabricating the components with different materials, with the number of steps usually corresponding to the number of used materials. This increases the fabrication time. Moreover, it requires the precise alignment of the structures and the fabrication of specific alignment markers for facilitating the process. Solutions to overcome such limitations have been proposed, exploiting custom-made microfluidic devices mounted on DLL substrates: microfluidic channels connected to pressure-flow control units allow delivering the desired materials in the writing area, i.e., different materials for fabrication, developers, and so on.<sup>[102,103]</sup> Alternatively, suspended rigid microstructures are obtained with a resolution higher than 100 nm by swelling a thermoresponsive poly(*N*-isopropylacrylamide) (PNIPAm) gel with acrylate monomer solution of IP-L 780 photoresist, as shown in **Figure 10b(i)**. The laser writing is performed inside the gel (in-gel DLL) and a freely designed structure is directly written into the gel, allowing the fabrication of suspended or fragile nonperiodic structures without any collapse, and supported by the solid substrate. This fabrication process creates an interpenetrating network of hydrogel and photoresist while preserving the properties of each material. The inscribed structure is thus like a skeleton that can direct volume changes in the gel (i.e., due to water uptake or increase in temperature) because of its cross-linking density, leading to controlled movements such as bending and distortion (**Figure 10b(ii)**).<sup>[104]</sup>

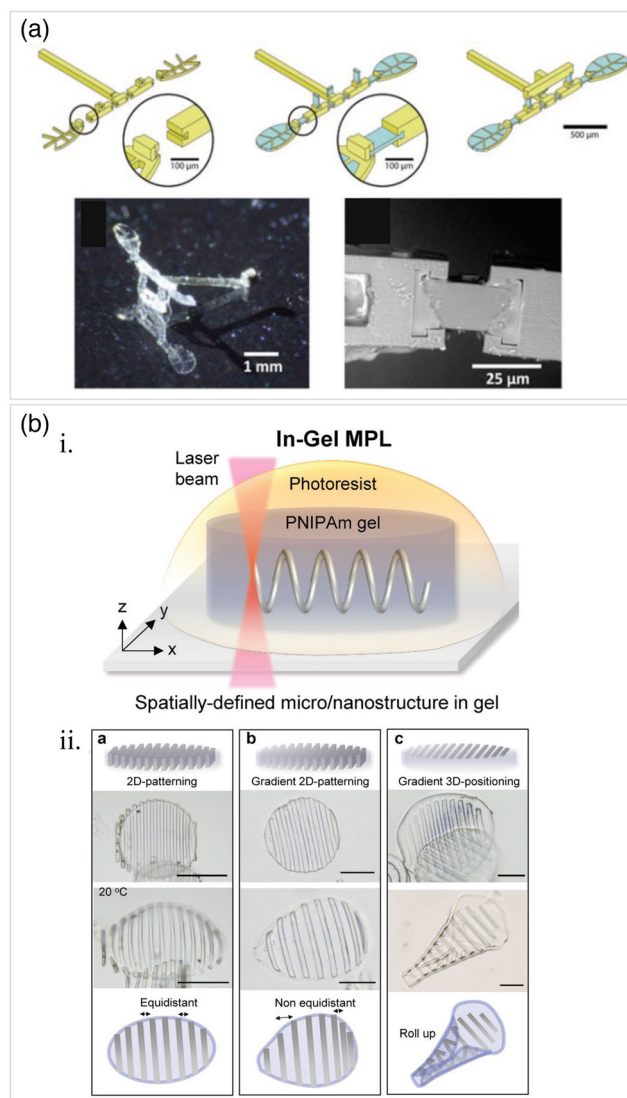


**Figure 10.** a) Schematic fabrication of the 2 mm wingspan flapping wing mechanism with flexible joints with rigid IPS parts (yellow) printed in the first and third step and flexible soft UDA components (light blue) printed in the second step (top). Photograph of the resulting structure and SEM image of the wing joint (bottom). Reproduced with permission.<sup>[101]</sup> Copyright 2020, Mary Ann Liebert, Inc. b) (i) Schematic of the in-gel DLL process; (ii) Design of structures patterned in PNIPAm gels and corresponding phase contrast images in water at 20 °C. Different behaviors are obtained with different designs. Reproduced with permission.<sup>[104]</sup> Copyright 2017, Wiley-VCH Verlag GmbH & Co. KGaA, Weinheim.

### 3.3.2. Cross-Linking Gradients in Stimuli-Responsive Materials based Microstructures

DLL can be used to tune the stiffness of specific sections of a microstructure, where the cross-linking gradients are locally predefined by varying the writing parameters (e.g., laser power, speed, and so on). This technique allows to overcome the drawbacks related to the multimaterial process, such as interlayer adhesion issues, that can arise at the micrometer scale.

However, it has to be considered that materials with very low cross-linking densities can achieve large deformations but can be too soft to be self-standing in 3D architectures. On the contrary, high cross-linking densities allow the fabrication of complex structures but with reduced deformability. Therefore, a trade-off is mandatory.

In recent years, because of the lack of active materials suitable for being processed by DLL, many custom-made photocurable materials have been developed having an intrinsic sensitivity to specific external stimuli such as pH (i.e. PAAc, PAAm), temperature (i.e. PNIPAAm), and light (i.e. azobenzene). Once the structure has been fabricated with such kind of materials, its 3D architecture can be further modified by changing the surrounding environment conditions in a 4D-DLL approach (i.e., application of a specific stimulus such as change in temperature or pH).<sup>[105–112]</sup> For example, self-propelled microrobots with microgripping and drug release capabilities are developed by combining pH- and photoresponsive materials.<sup>[106]</sup>

The sensitivity of these materials to the external stimulus changes in dependence of the cross-linking density, and complex actuation and sensing capabilities can be obtained. For example, in the study by Rekstyte et al.<sup>[113]</sup> the hybrid inorganic–organic photoresist SZ2080 is used for the fabrication of micromechanical structures that can be swelled by ethanol. The amount of solvent-induced deformation is based on the cross-linking density. The structures are composed of more rigid and densely cross-linked regions that are not subjected to swelling and thin deformable lines obtained with fewer scan passages of the laser for having a lower cross-linking of the material. In the presence of different amounts of ethanol in a water solution, the lines are able to deform and rotate around the rigid structure, forming different angles in dependence of the ethanol concentration in solution. Thus, the deformation can be used for microactuation or for sensing the proportion of ethanol and water. Thus, 4D DLL associated with variable stiffness microstructures opens the possibility to fabricate new generations of on-demand reconfigurable and self-morphing untethered microdevices and micromachines for applications in complex biological microenvironments (e.g., remotely minimally invasive operations, targeted drug delivery, cell manipulation, etc.). Indeed, coupling layers of the same material but different cross-linking density provides complex but controlled deformations. Bilayers can be assembled in 3D geometries forming the building blocks of more complex reconfigurable microstructures. Larger, complex, and continuum 3D to 3D shape transformations can be addressed through the assembly of these building blocks endowed with active deforming layers, rigid layers, and hinge joints, by following a programmable smart modular design.<sup>[105]</sup> In a very recent work, Jin et al.<sup>[110]</sup> develop a pH-sensitive photocurable material by adding both *N*-isopropyl acrylamide (NIPAAm; 98%) and acrylic acid functional monomers to an ethyl lactate solution. Then, PVP is used to adjust the photoresist viscosity, dipentaerythritol pentaacrylate (DPEPA) is added as cross-linker, triethanolamine (TEA) is used as a photosensitizer, and 4,4,0-bis(diethylamino)benzophenone (EMK) photoinitiator serves as gel precursor. Once exposed to the laser, the polymerized material shows shrinking and swelling behavior in acid and alkaline solutions, respectively. The sensitivity of the material to pH is tuned with the cross-linking level, and in particular lower sensitivity is observed at higher

densities (i.e., lower and higher levels of pH are required for shrinking or swelling respectively). Then, coupling layers of the same material but different density/crosslinking level, enables bending or rolling of the bilayered structure in response to pH variation because of the coupling of shrinking/swelling reactions. In the same work, a hollow microball with ten stripes distributed along its longitude is fabricated, with each strip divided into two layers: the outer one printed with high laser power (40 mW) and the inner one with a smaller laser power (12 mW) at the same velocity ( $8 \text{ mm s}^{-1}$ ). The variation of pH switches in a few seconds the microball shape back and forth between a spherical structure (swelling state) and a slender cylinder (shrinking state) because of the heterogeneous swelling and shrinking degree between the outer and inner layers of strips (Figure 11a). In the study b Huang et al.,<sup>[105]</sup> the same approach is used but, in this case, bilayers are assembled in 4D (i.e., time-deformable) building blocks (Figure 11b). Very complex deformable structures are then obtained by assembling such 4D building blocks in a modular mock-up that can change shape, e.g., a microscale race car transforming in a humanoid microrobot (Figure 11c).

This kind of self-shaping mechanism is very useful for fabricating innovative self-morphing machines at the microscale because their modification can be actuated and controlled wirelessly and on-demand. Also, the method does not require a manual assembly, which is not trivial at that scale. For example, in the study by Hu et al.<sup>[112]</sup> a pH-responsive hydrogel is used for the 4D printing of complex microcages developed to capture microparticles. Indeed, increasing the pH over the ionization threshold (pH = 9) causes the swelling of the polymer microparticles, which are captured because of the pore size change in the expanded/contracted states of the hexagonal microcages. When not swollen, the cage size is lower with respect to the microparticles size; the increase in pH causes pore expansion allowing microparticles to enter the cage. Then, by reducing pH the structures shrink again to their initial state, and the particles are trapped inside. The application of magnetic coatings allows for the transportation and remote targeted release of microparticles in a controlled way.

The use of sensitive materials with specific internal structure can also trigger color changes in addition to shape. As an example, in the work of del Pozo et al.,<sup>[111]</sup> 4D photonic microactuators with submicron resolution are fabricated with DLL using supramolecular cholesteric liquid crystalline (CLC) photonic photoresist. After base treatment, the structures show structural color and shape changes when exposed to a variation of humidity or temperature. Indeed, CLC network has a self-organized helical photonic structure that can selectively reflect light. Base treatment acts cleaving hydrogen bonds among specific molecules, resulting in a charged hygroscopic photonic polymer sensitive to changes in humidity and temperature. A variation of humidity causes the change of water vapor in air, directly inducing the structure to expand or contract. Alternatively, a change in temperature affects the rate of water evaporation, thus indirectly inducing the contraction (increase in temperature) or expansion (decrease in temperature) of the structure. Such controlled shape change induces a modulation of the nanoscale CLC pitch in the ordered network, and results in a corresponding color change

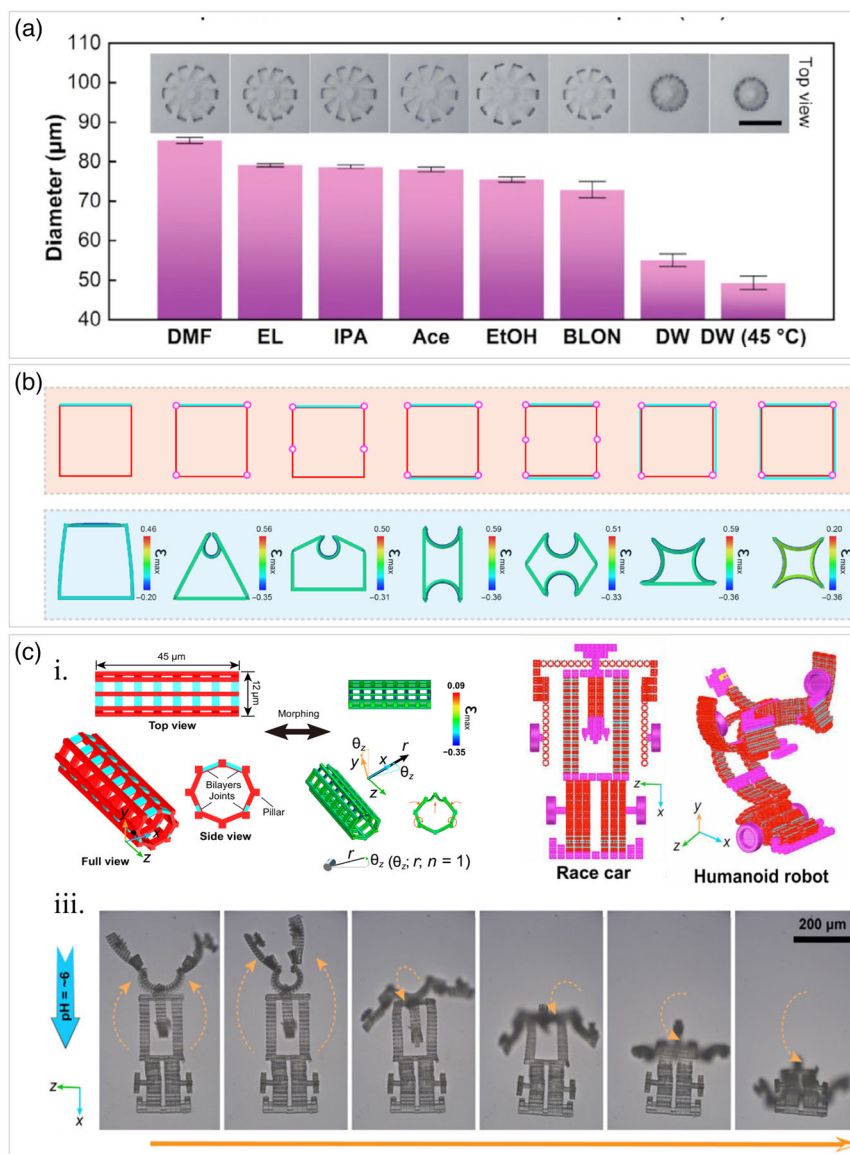


**Figure 11.** a) Graph reporting the effect of pH variation (induced by presence of solvent and temperature) on the diameter of a hollow microball fabricated with DLL. Solvents used: *N,N*-dimethylmethanamide (DNF), EL, IPA, Ace, EtOH, BLON, DW, and DW (45 °C) refer to *N,N*-dimethylmethanamide, ethyl lactate (EL), isopropanol (IPA), acetone (Ace), ethanol (EtOH), 1,4-butyrolactone (BLON), deionized water (DW) at room temperature, and at 45 °C (DW 45 °C). Scale bar of corresponding optical images: 60 μm. Reproduced with permission.<sup>[110]</sup> Copyright 1969, Elsevier. b) Simulations of transformations obtained for 4D building blocks fabricated with different arrangements of the bilayers and hinge joints. c) (i) Design of the 4D octagonal prismatic hollow cylinders structured with bilayers and hinge joints used as basic building blocks of a micro race car transforming in a humanoid robot through pH variation; (ii) optical images of the sequence of the transformation of the race car into a humanoid robot. The variation of pH is obtained with acidic fluid flow (diffusion direction is indicated by the blue arrow). Reproduced with permission.<sup>[105]</sup> Copyright 2020, Wiley-VCH Verlag GmbH & Co. KGaA, Weinheim.

that can be exploited for real-time evaluation of the status of microstructures, used as, e.g., microrobots.

### 3.3.3. Tuning of Mechanical Properties by Geometry

Geometry can play a prominent role in tuning the mechanical properties of microstructures to obtain specific functionalities, e.g., force sensing. Indeed, photosensitive resins are usually very

stiff ( $E \approx \text{GPa}$ ), but the design of specific architectures can give the structures an elastic behavior. For example, Alvo et al.<sup>[114]</sup> report the fabrication of microhelices (length 23–25 μm, pitch 4.5, diameter 4–4.8 μm, and thickness 0.6 μm) with DLL by using IPG 780 (Nanoscribe, GmbH) photoresist. The helical microstructures show a very high stiffness (mean value nearly  $0.82 \text{ N m}^{-1}$ ) when subjected to tensile elongation test (**Figure 12a**); however, they can elongate up to 39% in the linear range (68% in one case) and sustain forces from 4.2 up to

12.8  $\mu\text{N}$ . Therefore, the microdevice is suitable for force sensing at the microscale as also demonstrated in other works where a spring design has been adopted.<sup>[60,114,115]</sup>

Noteworthy, in another example,<sup>[116]</sup> a spring design is used for a microgripper with integrated force sensing. The gripper (with 100  $\mu\text{m}$  length and width) is fabricated with DLL using IP-Dip photoresist (Nanoscribe GmbH) directly on the tip of an optical fiber for simultaneous sensing and actuation (Figure 12b(i)). A supercontinuum laser source is connected to the optical fiber (with 125  $\mu\text{m}$  diameter) for illuminating the sensing part of the gripper. The optical sensor is composed of a series of four circular thin (1  $\mu\text{m}$ ) polymer platelets, arranged parallel along the vertical axis (with 10  $\mu\text{m}$  spacing), and supported by three springs (Figure 12b(ii)). At the end of the optical fiber, the broadband light is partially transmitted and reflected by the parallel plates, and the reflected light is collected back to a spectrometer. The obtained spectra are the readout of the compression state of the gripper, and thus, after a proper calibration it provides the force applied on the gripper. Indeed, when a normal force is applied, the springs compress causing changes in the distance between thin polymer plates and the subsequent change of the spectra. The design of the grippers with flexural hinges allows a compliant underactuated behavior; when an object approaches the palm of the grippers and applies a normal force the fingers close, leading to the gripping and holding of the object (Figure 12b(iii)). The force measurement error is minimal (0.79  $\mu\text{N}$ ), revealing how the fine tuning of the geometry enables a compliant design and accuracy of the force microsensors.

Force sensing is also crucial in mechanobiology research, and Klein et al.<sup>[117]</sup> pioneered the use of DLL in the field. Indeed, they used a biocompatible photoresist (Ormocomp, Micro Resist Technology, GmbH) to build a 3D web-shaped microstructure via DLL, composed of vertical pillars (15  $\mu\text{m}$  in height) connected by high aspect ratio horizontal beams with variable diameter

(0.66–1.33  $\mu\text{m}$ ) (Figure 13a). This specific design is used for sensing cellular traction forces. Unlike the pillars, the beams deform upon application of traction forces by cultured muscular cells (Figure 13b), which result in the range of tens of nN.

## 4. Conclusion

In this review, current trends in the DLL-based microfabrication of active microstructures are discussed. Taking DLL as a core enabling technology, the overall rationale is based on the different methodology to achieve active constructs, which is posited as indirect, when passive microstructures become active through postprocessing steps, or direct, when active structures are directly obtained by fabricating microstructures with active materials. In indirect methods, functionality is provided by the properties of the materials or biological components used in the postfabrication processing. Noteworthy, structures made out of nonphotosensitive materials can also be obtained by using passive structures as templates, molds, or masters. On the contrary, in direct methods functionality is given by the combination of two factors: the properties of the materials used for DLL (e.g., heterogeneous mechanical properties) and tuning of the laser writing parameters to create cross-linking gradients in stimuli-responsive materials. Here, postprocessing is usually not required.

However, in both cases, the design and fine control of geometrical parameters, enabled by DLL, play a fundamental role in controlling the functionality of the active structures. For example, in magnetically actuated microrobots, the material properties allow magnetic control, but choosing specific designs and dimensions enables a fine control of actuation parameters (e.g., velocity of microswimmers in biological fluids).<sup>[32,43]</sup> For sensing, among all cases the fine control on geometry is especially crucial in force microtransducers. Indeed, specific designs can be created only by

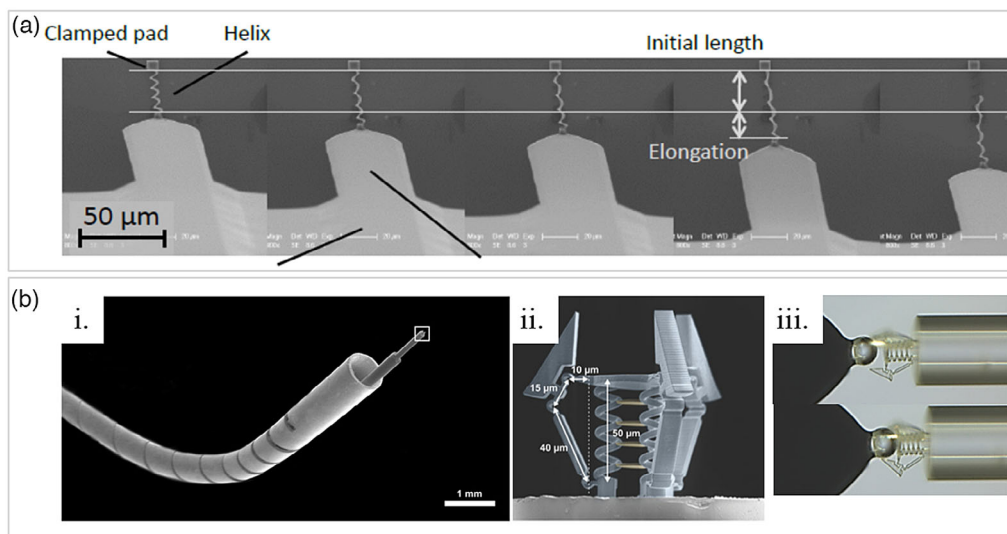


**Figure 12.** a) SEM images showing the sequence of the traction test performed on the microsprints. Reproduced with permission.<sup>[114]</sup> Copyright 2014, IEEE. b) (i) SEM image of the microgripper fabricated on top of an optical fiber inserted inside a catheter; (ii) SEM image of the microstructure integrating both gripping and sensing mechanism; (iii) optical images showing the gripper first approaching a MEMS force sensor (open uncompressed configuration, top) and then gripping the MEMS force sensor (closed configuration). Reproduced with permission.<sup>[116]</sup> Copyright 2018, Wiley-VCH Verlag GmbH & Co. KGaA, Weinheim.



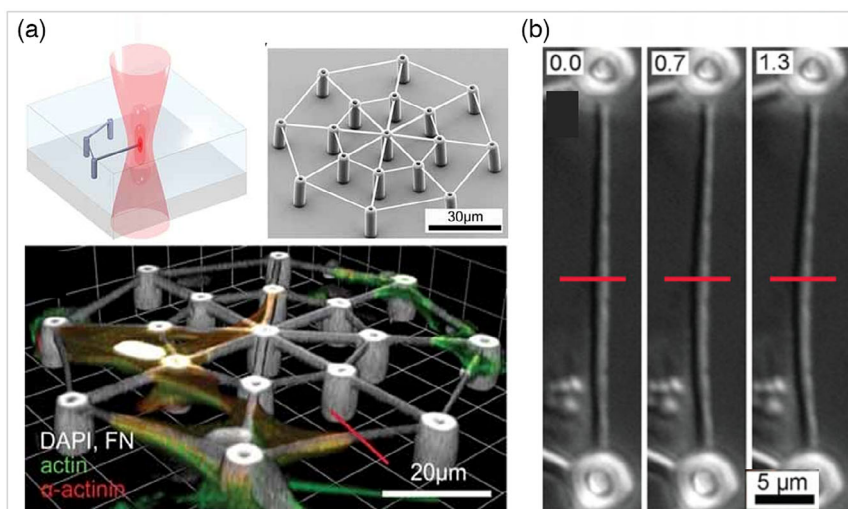


**Figure 13.** a) Scheme illustrating DLL fabrication of the web structure and SEM image of the obtained 3D scaffold and confocal image stack reconstruction of cells (i.e., cardiomyocytes) grown on the scaffold. b) Video frames of a beam deflected by a cell during contraction. Reproduced with permission.<sup>[117]</sup> Copyright 2010, Wiley-VCH Verlag GmbH & Co. KGaA, Weinheim.

DLL to achieve compliance by elastic structures at the microscale (e.g., microsprings).<sup>[114]</sup> The latter must suitably deform under the application of external forces, but need to be fabricated with stiff, reliable materials for avoiding collapsing when a force is applied. As reported in this review, unique spring-like force microsensors are obtained with both indirect and direct fabrication, e.g., by microsprings coated with a conductive material (i.e., CNTs)<sup>[49]</sup> and by optical-based sensing in a combined spring-plate microstructure,<sup>[116]</sup> respectively. In case of actuators, instead, soft materials are also used without compromising the efficiency of actuation but enhancing other properties, as in case of gelatin-based soft biodegradable hydrogel microstructures (i.e., GelMa microswimmers),<sup>[53,54]</sup> which provides a biocompatible substrate to support the neuronal cells growth, or multiple materials with very different mechanical characteristics (e.g., UDA and IPS) combined in the same structure are used integrated in a smart design for allowing complex actuation mechanisms.<sup>[101]</sup>

Indeed, in fabricating 3D active microstructures it is not always possible to clearly distinguish indirect and direct approaches, and in some cases their combination is needed to reach the desired functionality. For example, in the work of Hu,<sup>[112]</sup> microcages for the capture of microparticles are fabricated with pH-responsive hydrogel in a 4D printing approach (direct). However, targeted release is achieved only by deposition of a magnetic coating on the structures (indirect) and application of a magnetic rotating field.

Finally, in recent years researchers focused more on the development and optimization of stimuli-responsive materials to be used with DLL for achieving structures with specific functionalities, and material swelling linked to cross-linking is used for wirelessly controlled microactuation,<sup>[105,108,110]</sup> or for sensing environmental changes (e.g., sensing ethanol vs water) at the microscale in a 4D-DLL approach.<sup>[113]</sup> However, at the best of our knowledge, mechanical microsensing with soft materials still represents an open challenge that requires investigation on both materials and transducing approaches at the microscale.

## Supporting Information

Supporting Information is available from the Wiley Online Library or from the author.

## Conflict of Interest

The authors declare no conflict of interest.

## Keywords

3D printing, active materials, direct laser lithography, microdevices, multimaterial, photocurable materials, two-photon absorption

Received: March 18, 2021

Revised: May 8, 2021

Published online:

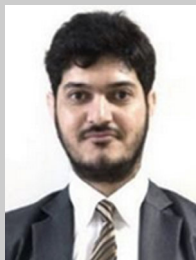
- [1] O. Tricinci, D. D. Pasquale, A. Marino, M. Battaglini, C. Pucci, G. Ciofani, *Adv. Mater. Technol.* **2020**, *5*, 2000540.
- [2] B. Ho, A. Mishra, K. Hu, J. An, Y.-J. Kim, Y. Yoon, *ACS Biomater. Sci. Eng.* **2017**, *3*, 2198.
- [3] M. M. Nava, T. Zandrini, G. Cerullo, R. Osellame, M. T. Raimondi, in *3D Cell Culture – Methods and Protocols* (Ed.: Z. Koledova), Springer, New York, NY **2017**, pp. 253–266.
- [4] M. T. Raimondi, S. M. Eaton, M. M. Nava, M. Laganà, G. Cerullo, R. Osellame, *J. Appl. Biomater. Funct. Mater.* **2012**, *10*, 55.
- [5] J. K. Gansel, M. Thiel, M. S. Rill, M. Decker, K. Bade, V. Saile, G. von Freymann, S. Linden, M. Wegener, *Science* **2009**, *325*, 1513.
- [6] J. K. Gansel, M. Latzel, A. Frölich, J. Kaschke, M. Thiel, M. Wegener, *Appl. Phys. Lett.* **2012**, *100*, 101109.
- [7] I. Sakellari, X. Yin, M. Nesterov, K. Terzaki, A. Xomalis, M. Farsari, *Adv. Opt. Mater.* **2017**, *5*, 1700200.
- [8] T. Blachowicz, A. Ehrmann, *Micromachines* **2020**, *11*, 434.
- [9] R. K. Jayne, T. J. Stark, J. B. Reeves, D. J. Bishop, A. E. White, *Adv. Mater. Technol.* **2018**, *3*, 1700293.

- [10] G. Tezel, S. Timur, F. Kuralay, R. Gürsoy, K. Ulubayram, L. Öner, H. Eroglu, *J. Drug Target.* **2020**, 29, 1.
- [11] R. Mishra, T. K. Maiti, T. K. Bhattacharyya, *J. Micromech. Microeng.* **2018**, 28, 105017.
- [12] G. Meloni, O. Tricinci, A. Degl'Innocenti, B. Mazzolai, *Sci. Rep.* **2020**, 10, 15480.
- [13] O. Tricinci, E. V. Eason, C. Filippeschi, A. Mondini, B. Mazzolai, N. M. Pugno, M. R. Cutkosky, F. Greco, V. Mattoli, *Smart Mater. Struct.* **2018**, 27, 075009.
- [14] Y. Cheng, *Micromachines* **2017**, 8, 59.
- [15] A. Alsharhan, R. Acevedo, R. Warren, R. Sochol, *Lab. Chip* **2019**, 19, 2799.
- [16] S. Maruo, J. t. Fourkas, *Laser Photonics Rev.* **2008**, 2, 100.
- [17] S. Kawata, H.-B. Sun, T. Tanaka, K. Takada, *Nature* **2001**, 412, 697.
- [18] R. Md. M. Hasan, X. Luo, *Nanomanuf. Metrol.* **2018**, 1, 67.
- [19] Y. Chen, *Microelectron. Eng.* **2015**, 135, 57.
- [20] S.-S. Kim, R. Chalykh, H. Kim, S. Lee, C. Park, M. Hwang, J. Park, P. Jinhong, H. Kim, J. Jeon, I. Kim, D. Lee, J. Na, J. Kim, S. Lee, H. Kim, S.-W. Nam, *Progress in EUV Lithography toward Manufacturing* (Ed: SPIE), The International Society for Optical Engineering, San Jose, CA, USA **2017**.
- [21] B. Bhushan, M. Caspers, *Microsyst. Technol.* **2017**, 23, 1117.
- [22] X. Wang, M. Jiang, Z. Zhou, J. Gou, D. Hui, *Compos. Part B Eng.* **2016**, 110, 442.
- [23] R. D. Farahani, M. Dubé, T. Daniel, *Adv. Mater.* **2016**, 28, 5794.
- [24] S. Maruo, O. Nakamura, S. Kawata, *Opt. Lett.* **1997**, 22, 132.
- [25] R. A. Farrer, C. N. LaFratta, L. Li, J. Praino, M. J. Naughton, B. E. A. Saleh, M. C. Teich, J. T. Fourkas, *J. Am. Chem. Soc.* **2006**, 128, 1796.
- [26] M. Thiel, J. Fischer, G. von Freymann, M. Wegener, *Appl. Phys. Lett.* **2010**, 97, 221102.
- [27] M. T. Do, T. T. N. Nguyen, Q. Li, H. Benisty, I. Ledoux-Rak, N. D. Lai, *Opt. Express* **2013**, 21, 20964.
- [28] D. T. T. Nguyen, M. T. Do, Q. Li, Q. CongTong, T. H. Au, N. D. Lai, *Theoretical Foundations and Application of Photonic Crystals*, IntechOpen, Rijeka **2017**.
- [29] S. Kang, K. Vora, E. Mazur, *Nanotechnology* **2015**, 26, 121001.
- [30] M. Thiel, M. Hermatschweiler, *Opt. Photonik* **2011**, 6, 36.
- [31] M. Carlotti, V. Mattoli, *Small* **2019**, 15, 1902687.
- [32] P. Liao, L. Xing, S. Zhang, D. Sun, *Small* **2019**, 15, 1901197.
- [33] J. Giltinan, P. Katsamba, W. Wang, E. Lauga, M. Sitti, *Appl. Phys. Lett.* **2020**, 116, 134101.
- [34] M. Kavaldzhiev, J. E. Perez, Y. Ivanov, A. Bertoncini, C. Liberale, J. Kosel, *Biomed. Phys. Eng. Express* **2017**, 3, 025005.
- [35] P. Liao, J. Li, S. Zhang, D. Sun, in *2018 IEEE Int. Conf. Robotics and Automation ICRA*, IEEE, Piscataway, NJ **2018**, pp. 3581–3586.
- [36] S. Jeon, S. Kim, S. Ha, S. Lee, E. Kim, S. Y. Kim, S. H. Park, J. H. Jeon, S. W. Kim, C. Moon, B. J. Nelson, J. Kim, S.-W. Yu, H. Choi, *Sci. Robot.* **2019**, 4, eaav4317.
- [37] S. Lee, S. Kim, S. Kim, J.-Y. Kim, C. Moon, B. J. Nelson, H. Choi, *Adv. Healthc. Mater.* **2018**, 7, 1700985.
- [38] J. Li, X. Li, T. Luo, R. Wang, C. Liu, S. Chen, D. Li, J. Yue, S. Cheng, D. Sun, *Sci. Robot.* **2018**, 3, eaat8829.
- [39] J. Li, W. Ma, F. Niu, Y. T. Chow, S. Chen, B. Ouyang, H. Ji, J. Yang, D. Sun, in *2016 IEEE Int. Conf. on Advanced Intelligent Mechatronics AIM*, IEEE, Piscataway, NJ **2016**, pp. 739–744.
- [40] S. Schuerle, A. P. Soleimany, T. Yeh, G. M. Anand, M. Häberli, H. E. Fleming, N. Mirkhani, F. Qiu, S. Hauer, X. Wang, B. J. Nelson, S. N. Bhatia, *Sci. Adv.* **2019**, 5, eaav4803.
- [41] S. Kim, S. Lee, J. Lee, B. J. Nelson, L. Zhang, H. Choi, *Sci. Rep.* **2016**, 6, 1.
- [42] S. Tottori, L. Zhang, F. Qiu, K. K. Krawczyk, A. Franco-Obregón, B. J. Nelson, *Adv. Mater.* **2012**, 24, 811.
- [43] Y. Chen, B. Xu, Y. Mei, *Chem. – An Asian J.* **2019**, 14, 2472.
- [44] L. Ren, N. Nama, J. M. McNeill, F. Soto, Z. Yan, W. Liu, W. Wang, J. Wang, T. E. Mallouk, *Sci. Adv.* **2019**, 5, eaax3084.
- [45] R. D. Baker, T. Montenegro-Johnson, A. D. Sediako, M. J. Thomson, A. Sen, E. Lauga, I. S. Aranson, *Nat. Commun.* **2019**, 10, 1.
- [46] X. Wang, C. Hu, L. Schurz, C. De Marco, X. Chen, S. Pané, B. J. Nelson, *ACS Nano* **2018**, 12, 6210.
- [47] C. A. Koepele, M. Guix, C. Bi, G. Adam, D. J. Cappelleri, *Adv. Intell. Syst.* **2020**, 2, 1900147.
- [48] D. Li, Y. Liu, Y. Yang, Y. Shen, *Nanoscale* **2018**, 10, 19673.
- [49] B. Li, B. Gil, M. Power, A. Gao, S. Teratanakulchai, S. Anastasova, G.-Z. Yang, *ACS Appl. Mater. Interfaces* **2019**, 11, 35577.
- [50] A. Barbot, D. Decanini, G. Hwang, *Int. J. Robot. Res.* **2020**, 39, 476.
- [51] T.-Y. Huang, M. S. Sakar, A. Mao, A. J. Petruska, F. Qiu, X.-B. Chen, S. Kennedy, D. Mooney, B. J. Nelson, *Adv. Mater.* **2015**, 27, 6644.
- [52] X. Xia, A. Afshar, H. Yang, C. M. Portela, D. M. Kochmann, C. V. Di Leo, J. R. Greer, *Nature* **2019**, 573, 205.
- [53] X. Wang, X.-H. Qin, C. Hu, A. Terzopoulou, X.-Z. Chen, T.-Y. Huang, K. Maniura-Weber, S. Pané, B. J. Nelson, *Adv. Funct. Mater.* **2018**, 28, 1804107.
- [54] M. Dong, X. Wang, X. Chen, F. Mushtaq, S. Deng, C. Zhu, H. Torlakcik, A. Terzopoulou, X. Qin, X. Xiao, J. Puigmartí-Luis, H. Choi, A. P. Pêgo, Q. Shen, B. J. Nelson, S. Pané, *Adv. Funct. Mater.* **2020**, 30, 1910323.
- [55] Y. Tao, C. Wei, J. Liu, C. Deng, S. Cai, W. Xiong, *Nanoscale* **2019**, 11, 9176.
- [56] H. Ceylan, I. C. Yasa, M. Sitti, *Adv. Mater.* **2017**, 29, 1605072.
- [57] H. Xu, M. Medina-Sánchez, V. Magdanz, L. Schwarz, F. Hebenstreit, O. G. Schmidt, *ACS Nano* **2018**, 12, 327.
- [58] H. Xu, M. M. Sanchez, V. Magdanz, L. Schwarz, F. Hebenstreit, O. G. Schmidt, arXiv:1703.08510.
- [59] P. Schürch, L. Pethö, J. Schwiedrzik, J. Michler, L. Philippe, *Adv. Mater. Technol.* **2018**, 3, 1800274.
- [60] P. Schürch, R. Ramachandramoorthy, L. Pethö, J. Michler, L. Philippe, *Appl. Mater. Today* **2020**, 18, 100472.
- [61] J. Askey, M. O. Hunt, W. Langbein, S. Ladak, *Nanomaterials* **2020**, 10, 429.
- [62] G. Williams, M. Hunt, B. Boehm, A. May, M. Taverne, D. Ho, S. Giblin, D. Read, J. Rarity, R. Allenspach, S. Ladak, *Nano Res.* **2018**, 11, 845.
- [63] C. C. J. Alcântara, S. Kim, S. Lee, B. Jang, P. Thakolkaran, J.-Y. Kim, H. Choi, B. J. Nelson, S. Pané, *Small* **2019**, 15, 1805006.
- [64] B. Jose, R. K. Vijayaraghavan, L. Kent, S. O'Toole, J. O'Leary, R. J. Forster, *Electrochem. Commun.* **2019**, 98, 106.
- [65] C. de Marco, C. C. J. Alcântara, S. Kim, F. Briatico, A. Kadioglu, G. de Bernardis, X. Chen, C. Marano, B. J. Nelson, S. Pané, *Adv. Mater. Technol.* **2019**, 4, 1900332.
- [66] I. Fiorello, F. Meder, O. Tricinci, C. Filippeschi, B. Mazzolai, in *Biomimetic and Biohybrid Systems* (Eds.: U. Martinez-Hernandez, V. Vouloutsis, A. Mura, M. Mangan, M. Asada, T. J. Prescott, P. F. M. J. Verschure), Springer International Publishing, Cham **2019**, pp. 122–133.
- [67] J. Giltinan, E. Diller, M. Sitti, *Lab Chip* **2016**, 16, 4445.
- [68] C. C. J. Alcântara, F. C. Landers, S. Kim, C. De Marco, D. Ahmed, B. J. Nelson, S. Pané, *Nat. Commun.* **2020**, 11, 5957.
- [69] J. Park, C. Jin, S. Lee, J.-Y. Kim, H. Choi, *Adv. Healthc. Mater.* **2019**, 8, 1900213.
- [70] H. Ceylan, I. C. Yasa, O. Yasa, A. F. Tabak, J. Giltinan, M. Sitti, *ACS Nano* **2019**, 13, 3353.
- [71] I. C. Yasa, A. F. Tabak, O. Yasa, H. Ceylan, M. Sitti, *Adv. Funct. Mater.* **2019**, 29, 1808992.
- [72] U. Bozuyuk, O. Yasa, I. C. Yasa, H. Ceylan, S. Kizilel, M. Sitti, *ACS Nano* **2018**, 12, 9617.

- [73] T. Komori, T. Komori, T. Furukawa, T. Furukawa, T. Furukawa, M. Iijima, S. Maruo, S. Maruo, *Opt. Express* **2020**, *28*, 8363.
- [74] T. Yamanaka, F. Arai, *Robomech. J.* **2019**, *6*, 22.
- [75] N. A. Bakhtina, N. MacKinnon, J. G. Korvink, in *Laser 3D Manufacturing III*, SPIE LASE, 2016, San Francisco, California, United States **2016**, Vol. 9738, pp. 97380C-97380C-10.
- [76] N. A. Bakhtina, A. Voigt, N. MacKinnon, G. Ahrens, G. Gruetzner, J. G. Korvink, in *2015 28th IEEE Int. Conf. on Micro Electro Mechanical Systems MEMS*, IEEE, Piscataway, NJ **2015**, pp. 97-101.
- [77] N. A. Bakhtina, U. Loeffelmann, N. MacKinnon, J. G. Korvink, *Adv. Funct. Mater.* **2015**, *25*, 1682.
- [78] Q. Hu, X.-Z. Sun, C. D. J. Parmenter, M. W. Fay, E. F. Smith, G. A. Rance, Y. He, F. Zhang, Y. Liu, D. Irvine, C. Tuck, R. Hague, R. Wildman, *Sci. Rep.* **2017**, *7*, 17150.
- [79] Y. Nakajima, K. Obata, M. Machida, A. Hohnholz, J. Koch, O. Suttmann, M. Terakawa, *Opt. Mater. Express* **2017**, *7*, 4203.
- [80] E. Blasco, J. Müller, P. Müller, V. Trouillet, M. Schön, T. Scherer, C. Barner-Kowollik, M. Wegener, *Adv. Mater.* **2016**, *28*, 3592.
- [81] S. Shukla, X. Vidal, E. P. Furlani, M. T. Swihart, K.-T. Kim, Y.-K. Yoon, A. Urbas, P. N. Prasad, *ACS Nano* **2011**, *5*, 1947.
- [82] A. Vyatskikh, S. Delalande, A. Kudo, X. Zhang, C. M. Portela, J. R. Greer, *Nat. Commun.* **2018**, *9*, 1.
- [83] N. Hauptman, M. Žvegljič, M. Maček, M. Klanjšek Gunde, *J. Mater. Sci.* **2009**, *44*, 4625.
- [84] J. Fischer, J. B. Mueller, J. Kaschke, T. J. A. Wolf, A.-N. Unterreiner, M. Wegener, *Opt. Express* **2013**, *21*, 26244.
- [85] W.-E. Lu, Y.-L. Zhang, M.-L. Zheng, Y.-P. Jia, J. Liu, X.-Z. Dong, Z.-S. Zhao, C.-B. Li, Y. Xia, T.-C. Ye, X.-M. Duan, *Opt. Mater. Express* **2013**, *3*, 1660.
- [86] T. Tanaka, A. Ishikawa, S. Kawata, *Appl. Phys. Lett.* **2006**, *88*, 081107.
- [87] A. Reiser, L. Koch, K. A. Dunn, T. Matsuura, F. Iwata, O. Fogel, Z. Kotler, N. Zhou, K. Charipar, A. Piqué, P. Rohner, D. Poulidakos, S. Lee, S. K. Seol, I. Utke, C. van Nesselroy, T. Zambelli, J. M. Wheeler, R. Spolenak, *Adv. Funct. Mater.* **2020**, *30*, 1910491.
- [88] Y.-Y. Cao, N. Takeyasu, T. Tanaka, X.-M. Duan, S. Kawata, *Small* **2009**, *5*, 1144.
- [89] B.-B. Xu, H. Xia, L.-G. Niu, Y.-L. Zhang, K. Sun, Q.-D. Chen, Y. Xu, Z.-Q. Lv, Z.-H. Li, H. Misawa, H.-B. Sun, *Small* **2010**, *6*, 1762.
- [90] P. Barton, S. Mukherjee, J. Prabha, B. W. Boudouris, L. Pan, X. Xu, *Nanotechnology* **2017**, *28*, 505302.
- [91] L. Liu, D. Yang, W. Wan, H. Yang, Q. Gong, Y. Li, *Nanophotonics* **2019**, *8*, 1087.
- [92] A. Ishikawa, T. Tanaka, S. Kawata, *Appl. Phys. Lett.* **2006**, *89*, 113102.
- [93] S. Maruo, T. Saeki, *Opt. Express* **2008**, *16*, 1174.
- [94] T. Baldacchini, A.-C. Pons, J. Pons, C. N. LaFratta, J. T. Fourkas, Y. Sun, M. J. Naughton, *Opt Express OE* **2005**, *13*, 1275.
- [95] C. N. LaFratta, D. Lim, K. O'Malley, T. Baldacchini, J. T. Fourkas, *Chem. Mater.* **2006**, *18*, 2038.
- [96] M. Machida, T. Niidome, H. Onoe, A. Heisterkamp, M. Terakawa, *Opt. Express* **2019**, *27*, 14657.
- [97] S. Arakane, M. Mizoshiri, J. Sakurai, S. Hata, *J. Micromech. Microeng.* **2017**, *27*, 055013.
- [98] M. Mizoshiri, S. Arakane, J. Sakurai, S. Hata, *Appl. Phys. Express* **2016**, *9*, 036701.
- [99] X.-L. Ren, M.-L. Zheng, F. Jin, Y.-Y. Zhao, X.-Z. Dong, J. Liu, H. Yu, X.-M. Duan, Z.-S. Zhao, *J. Phys. Chem. C* **2016**, *120*, 26532.
- [100] A. Astreinidi Blandin, I. Bernardeschi, L. Beccai, *Biomimetics* **2018**, *3*, 32.
- [101] M. Soreni-Harari, R. St. Pierre, C. McCue, K. Moreno, S. Bergbreiter, *Soft Robot.* **2019**, *7*, 59.
- [102] A. C. Lamont, M. A. Restaino, M. J. Kim, R. D. Sochol, *Lab. Chip* **2019**, *19*, 2340.
- [103] F. Mayer, S. Richter, J. Westhauser, E. Blasco, C. Barner-Kowollik, M. Wegener, *Sci. Adv.* **2019**, *5*, eaau9160.
- [104] A. Nishiguchi, A. Mourran, H. Zhang, M. Möller, *Adv. Sci.* **2018**, *5*, 1700038.
- [105] T.-Y. Huang, H.-W. Huang, D. D. Jin, Q. Y. Chen, J. Y. Huang, L. Zhang, H. L. Duan, *Sci. Adv.* **2020**, *6*, eaav8219.
- [106] M. Power, S. Anastasova, S. Shanel, G.-Z. Yang, in *2017 IEEE Int. Conf. on Robotics and Automation ICRA*, IEEE, Piscataway, NJ **2017**, pp. 6002-6007.
- [107] L. D. Zarzar, P. Kim, M. Kolle, C. J. Brinker, J. Aizenberg, B. Kaehr, *Angew. Chem., Int. Ed.* **2011**, *50*, 9356.
- [108] M. Hippler, E. Blasco, J. Qu, M. Tanaka, C. Barner-Kowollik, M. Wegener, M. Bastmeyer, *Nat. Commun.* **2019**, *10*, 232.
- [109] C. Lv, X.-C. Sun, H. Xia, Y.-H. Yu, G. Wang, X.-W. Cao, S.-X. Li, Y.-S. Wang, Q.-D. Chen, Y.-D. Yu, H.-B. Sun, *Sens. Actuators, B* **2018**, *259*, 736.
- [110] D. Jin, Q. Chen, T.-Y. Huang, J. Huang, L. Zhang, H. Duan, *Mater. Today* **2020**, *32*, 19.
- [111] M. del Pozo, C. Delaney, C. W. M. Bastiaansen, D. Diamond, A. P. H. J. Schenning, L. Florea, *ACS Nano* **2020**, *14*, 9832.
- [112] Y. Hu, Z. Wang, D. Jin, C. Zhang, R. Sun, Z. Li, K. Hu, J. Ni, Z. Cai, D. Pan, X. Wang, W. Zhu, J. Li, D. Wu, L. Zhang, J. Chu, *Adv. Funct. Mater.* **2020**, *30*, 1907377.
- [113] S. Rekstyte, D. Paipulas, V. Mizeikis, *Nanotechnology* **2017**, *28*, 124001.
- [114] S. Alvo, D. Decanini, L. Couraud, A.-M. Haghiri-Gosnet, G. Hwang, in *2014 IEEE/RSJ Int. Conf. on Intelligent Robots and Systems*, IEEE, Piscataway, NJ **2014**, pp. 4656-4661.
- [115] S. Ushiba, K. Masui, N. Taguchi, T. Hamano, S. Kawata, S. Shoji, *Sci. Rep.* **2015**, *5*, 1.
- [116] M. Power, A. J. Thompson, S. Anastasova, G.-Z. Yang, *Small* **2018**, *14*, 1703964.
- [117] F. Klein, T. Striebel, J. Fischer, Z. Jiang, C. M. Franz, G. Von Freymann, M. Wegener, M. Bastmeyer, *Adv. Mater.* **2010**, *22*, 868.
- [118] S. Lee, J. Kim, J. Kim, A. K. Hoshier, J. Park, S. Lee, J. Kim, S. Pané, B. J. Nelson, H. Choi, *Adv. Healthc. Mater.* **2020**, *9*, 2070019.
- [119] F. Formanek, N. Takeyasu, T. Tanaka, K. Chiyoda, A. Ishikawa, S. Kawata, *Opt. Express* **2006**, *14*, 800.
- [120] K. Terzaki, N. Vasilantonakis, A. Gaidukeviciute, C. Reinhardt, C. Fotakis, M. Vamvakaki, M. Farsari, *Opt. Mater. Express* **2011**, *1*, 586.
- [121] T. Jonavičius, S. Rekštytė, A. Žukauskas, M. Malinauskas, in *Laser 3D Manufacturing*, International Society for Optics and Photonics, Bellingham, WA **2014**, p. 89700C.
- [122] K. Kurselis, R. Kiyani, V. N. Bagratashvili, V. K. Popov, B. N. Chichkov, *Opt. Express* **2013**, *21*, 31029.
- [123] A. J. Thompson, M. Power, G.-Z. Yang, *Opt. Express* **2018**, *26*, 14186.



**Irene Bernardeschi** is a postdoc in the Soft BioRobotic Perception research line of Istituto Italiano di Tecnologia (Genova, Italy). She received her Ph.D. in Innovative Technologies – curriculum Biorobotics at the Scuola Superiore Sant’Anna (Pisa, Italy) in 2015. Her main scientific interests include the study of natural models for the development of bioinspired 2D and 3D soft and stretchable sensors at different scales (from micro- to macroscale) for applications in soft robotics, with a focus on tactile sensing, wearable devices and related technologies. Her work is focused on natural/artificial material investigation and characterization and fabrication strategies development.



**Muhammad Ilyas** is a postdoctoral researcher in the Soft BioRobotic Perception research line of the Istituto Italiano di Tecnologia (Genova, Italy). He received his Ph.D. in Transdisciplinary Life Science majoring in Polymers and Materials Science at the Laboratory of Soft and Wet Matter, Graduate School of Life Science, Hokkaido University (Japan) in 2018. His research interests are in biomimetic 3D mechanical sensors at different length scales ranging from micro- to macroscale for tactile sensing application. His research is focused on the investigation, synthesis formulation/development, fabrication, characterization of soft smart multifunctional materials, and 2D, 3D, 4D printing of soft materials.



**Lucia Beccai**, Ph.D. is Tenured Senior Researcher at the Istituto Italiano di Tecnologia (Genova, Italy), where she leads the group *Soft BioRobotic Perception*. She has a long experience in bioinspired smart tactile systems and bionics. She is interested in soft and embodied sensing processes, with a focus on touch, to enable soft perceptive robots of natural-like physical interactions, like in bioinspired soft grasping and manipulation. Currently she is the coordinator of the PROBOSCIS project (EU H2020-FET Open 863212). She filed 3 patents and she is author of more than 100 articles on refereed international journals, books, and international conference proceedings.